A METHOD FOR ESTIMATING TARGET VELOCITY AND RANGE WITH PASSIVE SEEKER DATA

BUĞRA CAN BABAOĞLU

JANUARY 2018

A METHOD FOR ESTIMATING TARGET VELOCITY AND RANGE WITH PASSIVE SEEKER DATA

A THESIS SUBMITTED TO
THE GRADUATE SCHOOL OF NATURAL AND APPLIED SCIENCES
OF
MIDDLE EAST TECHNICAL UNIVERSITY

BY

BUĞRA CAN BABAOĞLU

IN PARTIAL FULFILLMENT OF THE REQUIREMENTS
FOR
THE DEGREE OF MASTER OF SCIENCE
IN
AEROSPACE ENGINEERING

JANUARY 2018

Approval of the thesis:

A METHOD FOR ESTIMATING TARGET VELOCITY AND RANGE WITH PASSIVE SEEKER DATA

submitted by **BUĞRA CAN BABAOĞLU** in partial fulfillment of the requirements for the degree of **Master of Science in Aerospace Engineering Department, Middle East Technical University** by,

Prof. Dr. Gülbin Dural Ünver _____
Dean**,** Graduate School of **Natural and Applied Sciences**

Prof. Dr. Ozan Tekinalp _____
Head of Department**, Aerospace Engineering**

Asst. Prof. Dr. Ali Türker Kutay _____
Supervisor**, Aerospace Engineering Dept., METU**

Examining Committee Members

Prof. Dr. Ozan Tekinalp _____
Aerospace Engineering Dept., METU

Asst. Prof. Dr. Ali Türker Kutay _____
Aerospace Engineering Dept., METU

Assoc. Prof. Dr. İlkay Yavrucuk _____
Aerospace Engineering Dept., METU

Prof. Dr. Kemal Leblebicioğlu _____
Electrical and Electronics Engineering Dept., METU

Asst. Prof. Dr. Yakup Özkazanç _____
Electrical and Electronics Engineering Dept.,
Hacettepe University

Date: _____

I hereby declare that all information in this document has been obtained and presented in accordance with academic rules and ethical conduct. I also declare that, as required by these rules and conduct, I have fully cited and referenced all material and results that are not original to this work.

Name, Last Name **:** BUĞRA CAN BABAOĞLU

Signature **:**

ABSTRACT

A METHOD FOR ESTIMATING TARGET VELOCITY AND RANGE WITH PASSIVE SEEKER DATA

Babaoğlu, Buğra Can

M.S., Department of Aerospace Engineering

Supervisor: Assist. Prof. Dr. Ali Türker Kutay

January 2018, 78 pages

In basic guidance applications, the line-of-sight (LOS) and line-of-sight rate information, which can be provided using a passive seeker, are enough to steer the missile to the target. However, if one wants to augment the guidance algorithm, further information regarding the engagement and/or target is needed. Unlike passive seekers, active and semi-active seekers may provide such information. Nevertheless, if the missile is equipped with a passive seeker, those parameters need to be estimated. Various methods are available in the literature for the estimation, which use Kalman Filters, lacking observability if the missile does not accelerate. In this thesis, using a brute force method, a new algorithm for estimating target parameters is proposed; which does not need missile acceleration for observability.

Keywords: Range Estimation, Passive Seeker, Velocity Estimation

ÖZ

EDİLGEN ARAYICILI SİSTEMLER İÇİN BİR HEDEF HIZI VE MENZİL KESTİRİMİ YÖNTEMİ

Babaoğlu, Buğra Can

Yüksek Lisans, Havacılık ve Uzay Mühendisliği Bölümü

Tez Yöneticisi: Yrd. Doç. Dr. Ali Türker Kutay

Ocak 2018, 78 sayfa

Temel güdüm uygulamalarında, bir edilgen arayıcı tarafından sağlanan görüş hattı açısı (LOS) ve görüş hattı açısal hızı bilgileri bir füzeyi hedefe yönlendirmek için yeterlidir. Ancak, tasarımcı güdüm algoritmalarını geliştirmek ister ise angajman ve/veya hedef ile ilgili bilgiye ihtiyacı vardır. Edilgen arayıcıların aksine, etkin ve yarı etkin arayıcılar bu parametreleri sağlayabilir. Ancak, füze üzerinde edilgen bir arayıcı mevcut ise, bu parametrelerin kestirilmesi gerekir. Literatürde konuyla ilgili birtakım yöntemler mevcut olup, bunlar ekseriyetle Kalman Filtresi yöntemini kullanırlar. Bu yöntemlerle tasarlanmış filtreler, füze manevrasının olmadığı durumlarda gözlemlenebilirliğini kaybetmektedir. Bu tezde, bir kaba kuvvet yöntemi ile geliştirilmiş, gözlemlenebilirlik için füze manevrasına gerek duymayan bir hedef ve angajman parametreleri kestirimi algoritması sunulmuştur.

Anahtar Kelimeler: Menzil Kestirimi, Edilgen Arayıcı, Hız Kestirimi

pour les nouveaux débuts

ACKNOWLEDGMENTS

I would like to express my gratitude to my supervisor Asst. Dr. Ali Türker Kutay for creating a free environment for my studies and being helpful and understanding during my thesis work. I was always welcomed when I needed assistance.

I also would like to thank Assoc. Dr. Tayfun Çimen for his academic and friendly support. His help was very crucial for me. I am hoping to continue working with him in my academic career.

I am also very lucky to have the supports of Naz Tuğçe Öveç, Görkem Eşsiz and Suzan Kale Güvenç as my co-workers and friends. I would like to express my special thanks to Akif Altun for being so open-handed (especially his gas expenditure and time consumption) and his helpful nature.

I am forever indebted to my parents, Cafer Babaoğlu, Dilek Babaoğlu and my brother Bora Babaoğlu for being there for me all the time, whenever I needed, wherever I needed, unquestionably. Likewise, I am so lucky to have all my grandparents, aunts, uncles and cousins as they were always supportive.

Last, but not least, I cannot express how lucky I am to have my love and everything, Sogand Yousefbeigi, for being so supportive and caring – and for just being there, which I could never pay off in my entire life.

TABLE OF CONTENTS

LIST OF FIGURES

FIGURES

LIST OF TABLES

TABLES

CHAPTER 1

INTRODUCTION

1.1. Basics

A guided missile can be defined as a type of munition where the missile is directed towards a target by means of calculated routing commands. These commands incorporate target-missile kinematics of which variables are measured through either on-board or external sensors. The variables that consist target-missile kinematics include, but not limited to *line-of-sight*, *range*, *closing velocity* etc. The process (or algorithm) of calculating the routing commands from those variables is called *Guidance Law* [1].

One of the oldest application of such a law is called *Parallel Navigation* (or *Collusion Course*), which was especially common in old maritime applications [1] [2] where pirates attempt to seize a merchant ship by maintaining constant bearing. If such bearing was met, and the target ship was getting larger in sight; than it was said that both ships are on a collision course and they eventually meet at some point. Similarly, rodents use parallel navigation techniques to reach their targets, depending on the task itself [3].

In most modern missile application, similar to parallel navigation, a common law called *Proportional Navigation Guidance* (PNG) is used [4]. This law states that, the steering commands should be proportional to the line of sight rate (Elaborated in following chapters) which is the only measurement required regarding the target and engagement.

1.2. Motivation

PNG is the most common guidance law that is currently being implemented in the industry. It is considered satisfactory when the total engagement time is relatively long when compared to the rise time of the guidance loop and missile is capable of performing higher manoeuvres compared to the target [5]. Nevertheless, PNG is a successful or the optimal solution among other methods under some assumptions like constant closing velocity, non-existent missile dynamics etc. Also, along with high sensitivity to input noise, increased technology within the target portfolio of missiles aggravate the performance of PNG [1] [4]. Better modelling of target motion is needed in order to increase the capability of the missile. For that end, more information about target and engagement (target velocity, range etc.) is required.

Moreover, modern guidance applications now require more advanced solutions like optimal guidance [6], impact time constraint [7] [8], impact angle constraint [9] etc. The common thing in [6] - [9] is that, they all need extra engagement and/or target information besides LOS rate; like *time-to-go* or target velocity.

The aforementioned requirements cause problem from two different aspects (elaborated in following chapters):

- Measurement of those variables requires active tracking; increasing the risk of being detected by the target
- Not having the required equipment to actively track the target due to weight and/or other physical limitations

Especially for small munitions, the physical limitations are a critical parameter. Hence, they are equipped with passive seekers.

In such cases, the only available measurements regarding the engagement are generally LOS and LOS rate, which are enough for standard PNG applications but not sufficient for more advanced tasks. Therefore, it is a field of study to estimate other parameters like range and target velocity.

1.3. Literature Review

Estimating target and engagement parameters using LOS and LOS rate only is called "*angle-only target tracking*" in the literature ("*bearings only tracking*" is also available).

Estimating the position of a point in space is a custom application in various fields, including geodesy, maritime warfare etc [10]. During World War II, the British were interested in finding an accurate target position using two or more D.F. (direction finding) stations [11] [12].

One of the algorithms used to estimate the position of a target is called *Triangulation*. This simple method is applicable to stationary targets. In such a case, if the angular position of the target relative to the missile and position of the missile is known at two different time steps; the position of the target can be computed by simple geometry. However, this method is vulnerable to measurement errors. To tackle this problem, noise characteristics of the measurements should be taken into consideration, as suggested in [13].

In most modern applications of target estimation, Kalman Filter and its different versions are the primary choice. The fundamentals of Kalman Filters are readily available in the literature [14], [15]. Since the tracking problem has a nonlinear nature [16], rather than plain Kalman Filter, Extended Kalman Filter (EKF) or Unscented Kalman Filter (UKF) are currently being used in the literature. For example, in [17], a regular Kalman Filter is proposed. Whereas in [18], an EKF is proposed by augmenting the model proposed in [17].

In those methods, observer acceleration is mandatory in order to have an observable solution [19] [20]. The observability problem can be considered as the hot topic of these algorithms. The issue is addressed in several publications including [21], [22]. To remedy the observability problem, in [23] and [24], which proposes certain guidance methods (called *Modified Proportional Navigation Guidance* or *Target Adaptive Guidance*) to save observability by changing the guidance structure; which also requires information related to target and engagement.

1.4. Contributions

A new algorithm for both target speed and range estimation, which does not utilize Kalman Filter is proposed. A brute force approach is presented, the physical limitations of the missile-target engagement are exposed.

In the proposed algorithm, missile manoeuvre is not necessary for observability as opposed to Kalman filter applications. It is shown that, the only condition for observability for this algorithm is a non-zero LOS rate, which should be attained only when the algorithm is initiated. This enables the algorithm to be used in any midcourse guidance phase where the missile does not manoeuvre much or does not manoeuvre at all.

If Kalman Filter (or EKF, UKF etc.) is used, a good initial estimate is an important factor of the stability of the filter [25]. The proposed algorithm does not suffer from this drawback, as it does not need any initial estimate; it rather needs pre-determined elements (which could be adapted during flight – elaborated in Future Works), which are physically bounded.

Since the algorithm does not use any dynamic modelling (system matrix, covariance matrix, Kalman gains etc.), instability can be discarded as a problem. If the algorithm starts providing gibberish results, it can be reset easily since initialization is not a hard issue.

How the small deviations in measurements can affect the estimations are also investigated by algebraic manipulations and simulation results.

1.5. Outline

The remainder of the thesis is organized as follows:

- In Chapter 2, the basic concepts of *Guidance*, *Guidance Loop*, *Seeker*, *LOS*, *Engagement Geometry* and their mathematical representations are presented to provide a background.
- In Chapter 3, the proposed algorithm and related mathematical expressions are presented. The *synthetic* concept is explained. Moreover, the consequences of having errors in measurements are also shown.

- In Chapter 4, the simulation environment is presented. Simulation conditions and how the real-world effects are included to the environment. Then, the parameters related to the algorithm are shown
- In Chapter 5, the algorithm is tested in various conditions in the environment described in Chapter 4; starting with an ideal case, where every measurement is perfect. Then, errors added to the simulation to investigate the effects of them. The discussion related to those results are presented following each test. The effects of imperfections are investigated. Also, a batch run in which a wide space of scenarios are tested is presented.
- In Chapter 6, the discussion is concluded with some remarks about future works that could make the algorithm better and more practical.

CHAPTER 2

MISSILE GUIDANCE & ENGAGEMENT GEOMETRY

In this chapter, basic concepts related to missile and missile algorithms are presented. Then the geometry created by the missile and target and its mathematical formulation is shown. Finally, the mathematical expressions related to engagement geometry are interpreted in a passive seeker point of view, which would establish a background for the proposed algorithm.

2.1. Missile Fundamentals

In Oxford Living Dictionary [26] missile is defined as "*An object which is forcibly propelled at a target, either by hand or from a mechanical weapon*". From guidance point of view, the main purpose of a missile is to reach a certain target, within its flight envelope. To that end, missiles are equipped with certain algorithms, which directs the missile to its target.

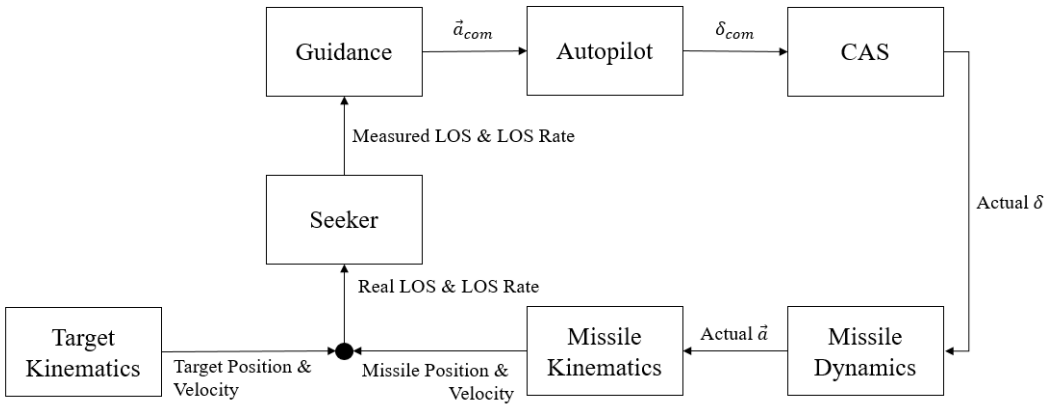

Figure 2.1. A typical guidance loop in a missile

A simple guidance loop where sensors are omitted is illustrated in Figure 2.1. *Guidance*, *Autopilot* and *CAS* are the main elements of a missile algorithm of which tasks are elaborated in section Missile Algorithms.

Along with algorithms, missiles are also equipped with certain sensors which provide the necessary data to be used in algorithms.

Inertial Measurement Unit, also known as *IMU,* is an inertial sensor, consisting of gyroscopes (measuring angular rates) and accelerometers (measuring translational accelerations). Its outputs are the inputs of various algorithms like navigation, autopilot, guidance etc.

Seeker is a key element for guidance algorithms since it provides the LOS and LOS rate data. There are three class of seekers in terms of homing type [27].

1) *Active seekers* send active signals to the target and detects the target by reading returning signals. Actively sending signals, enables the missile to directly obtain the range to the target along with LOS and LOS rate data. However, they require more weight, space, cost and the risk of detection due to its active nature.
2) *Semi-Active seekers,* are similar to active ones. The difference is that, the seeker (e.g. radar) is not mounted on the missile itself, it is located at a different location like, ground, firing ship or aircraft etc.
3) *Passive seekers*, which are also the focus of this theses, detects the signals emitted by the target. For example, an infrared seeker (IR seeker) detects the heat signature of the target. Since they do not use any active signals, they cannot be detected as easy as active seekers. However, passive seekers are unable to estimate the range to target (or the target velocity); they can only provide LOS and LOS rate data.

2.2. Missile Algorithms

2.2.1. Autopilot

Main duty of an autopilot is to calculate the necessary fin deflections angles that CAS should realise in order to sustain the guidance commands that steers the missile to its

target. Various autopilot algorithms are available in the literature, which are out of the scope of this thesis.

2.2.2. Control Actuation System

Control Actuation System (or CAS) is a mechanism which includes fins that causes acceleration when their angles are changed, DC motors (or other actuation device like pneumatics) which changes the angles of the fins and an algorithm to drive the DC motors. The main purpose of CAS is to perform the angle commands created by the autopilot.

2.2.3. Guidance

The essential duty of a guidance algorithm is to *interpret* the current situation of the engagement kinematics, and provide the required commands to the autopilot. The most widely used guidance algorithm is called *Proportional Navigation Guidance* (PNG) where LOS rate and missile velocity is used as inputs and acceleration command is produced as output, as depicted in (2.1).

$$\vec{a}_{com} = N\vec{\lambda} \times \vec{v}_m \tag{2.1}$$

In (2.1), $\vec{\lambda}$ is the LOS angular rate vector, provided by the seeker, $\vec{v}_m$ is the missile velocity vector, calculated using IMU outputs, N is called *PNG Gain*, a value larger than 2. PNG algorithms can be "augmented" by incorporating several other variables like time-to-go and range [27] which are unavailable where the seeker is passive.

2.3. Engagement Geometry

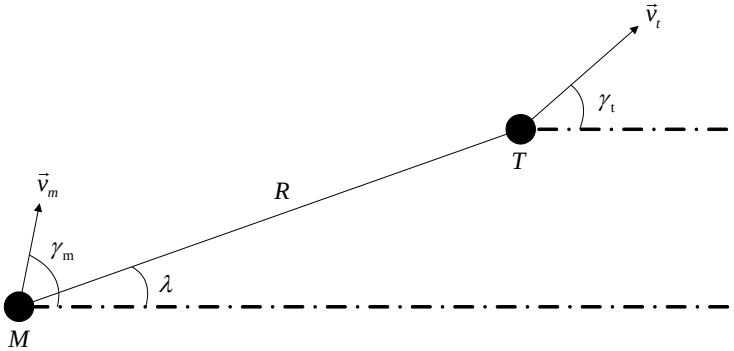

Figure 2.2. Typical 2D engagement geometry

An engagement geometry is the resultant geometry due to the interaction of missile and target. Figure 2.2 depicts a 2D engagement geometry, which is the main scope of the work in this thesis. In the figure, $\vec{v}_m$ and $\vec{v}_t$ are the missile and target velocities; γ_m and γ_t are missile and target flight path angles, R is range and λ is the line-of-sight angle.

The kinematics of the engagement geometry is driven by two scalar equations. One equation drives the angular position (2.2), and the other drives the translational position (2.3) of the relative kinematics.

$$\dot{\lambda} = \frac{V_m \sin(\lambda - \gamma_m) - V_t \sin(\lambda - \gamma_t)}{R} \tag{2.2}$$

$$\dot{R} = -V_m \cos(\lambda - \gamma_m) + V_t \cos(\lambda - \gamma_t) \tag{2.3}$$

In (2.2) and (2.3), V_m and V_t are the scalar values of the missile and target speeds, respectively. Consequently, the following remarks can be made:

- There are four unknowns (V_t, γ_t, R, $\dot{R}$) with two equations. (2.2) and (2.3) cannot be solved algebraically. There is a deficit of two unknowns.
- (2.2) has also deficit of two unknowns (one equation, three unknowns). When (2.3) is added alongside with (2.2), it does not change the deficit level (two) as it introduces another unknown ($\dot{R}$).
- If range was known perfectly, its derivative with respect to time can be taken and the aforementioned equation system can be solved
- When the target is stationary ($V_t = 0$), both R and $\dot{R}$ can directly be found.

Consequently, the complete knowledge of the engagement geometry requires either one of the following:

- Stationary target
- Perfect (differentiable) knowledge of range
- Knowledge of two of the unknowns

Since the existence of a stationary target cannot be guaranteed, and perfect knowledge of range (or any measurement) is impractical; estimation of target and/or engagement parameters is a more practical method, which is the focus of thesis.

CHAPTER 3

ESTIMATION ALGORITHM

3.1. Mathematical Background

The basis of the algorithm is constructed from (2.2). Rearranging gives:

$$R = \frac{V_m \sin(\lambda - \gamma_m) - V_t \sin(\lambda - \gamma_t)}{\dot{\lambda}} \tag{3.1}$$

In (3.1), one thing that should be noted is that, the unknowns on the right-hand side of the equation (γ_t & V_t) are physically bounded. Namely, target flight path angle values range from 0 to 360°. Likewise, target speed values range from zero up to a certain limit. That limit can be enforced by the duty of the missile; in other words, it can be considered as unnecessary to estimate a target which cannot be captured by the missile. For example, an anti-tank missile can only capture a tank of which speed is limited and its limit is known prior to algorithm design.

Therefore, it can be said that, *guessing* the target velocity *vector* successfully, which is bounded by physical limits, is sufficient to calculate range from (3.1). Consequently, the problem becomes guessing the target velocity vector as good as possible.

Note that in (3.1), it can be seen that, whenever the LOS rate value is zero, the division becomes impractical, yielding in an unobservable situation. Thus, the only engagement criterion for observability becomes a non-zero LOS rate value.

3.1.1. Uniqueness Problem

It was said that for a missile with passive seeker, engagement geometry equations have an unknown deficit of two. This means that, there are infinite number of solutions

at a specific time point.

Figure 3.1 depicts the aforementioned uniqueness problem. Without the information of range and/or target velocity, despite the knowledge of missile velocity and LOS angles (and LOS rates), target movement could either be from T_1 to T_2 or T_1' to T_2' (or one of the infinitely many displacements not depicted in Figure 3.1), where M_1 and M_2 represents missile position in consecutive timesteps.

Therefore, it is impossible to find a solution within a single timestep as there are infinitely many solutions for the problem due to the lack of information about the engagement. Consequently, the algorithm aims to look at the problem within a period of time.

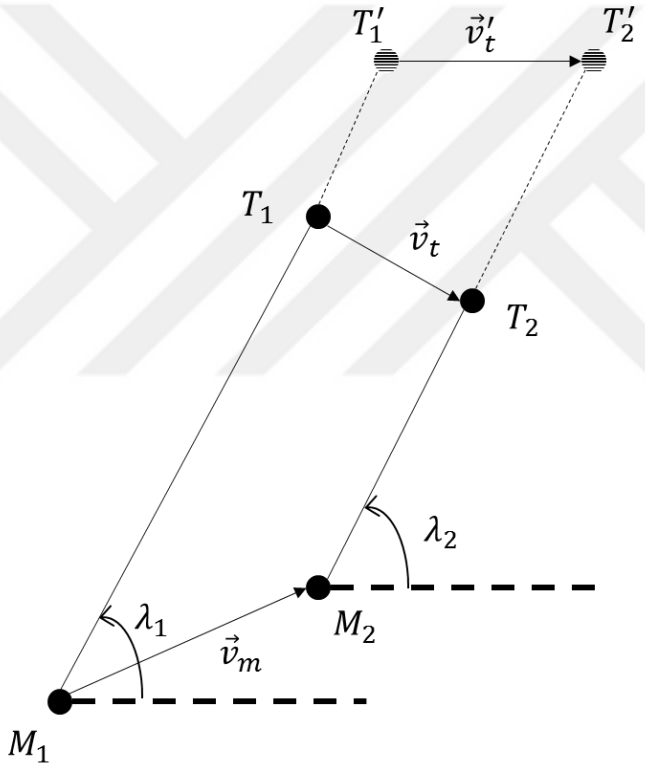

Figure 3.1. Uniqueness problem in an engagement

3.2. Search Space Creation

In this section, creation of a so-called *search space*, the domain of interest where the estimation algorithm would search for the correct estimate is defined and its construction is explained.

3.2.1. Guess Couples & Guessed Position Matrix

To correctly estimate the engagement geometry, as previously stated, it is sufficient to correctly guess the target velocity vector consisting of a scalar speed value (V_t) and a scalar angle value (γ_t). Bearing in mind that these values are physically bounded, a "*search space*" is created.

A *search space* consists of a number of *guess couples* which are created by speed and angle guesses, depicted as $\hat{V}_{t_i}$ (i^{th} guess of V_t) and $\hat{\gamma}_{t_j}$ (j^{th} guess of γ_t). By doing so, current real engagement geometry would enforce a range guess ($\hat{R}_{ij}$) through (3.1) for each guess couple. So, using the calculated range guess and known LOS angle, the position of the target can be guessed using (3.2) where x_m and z_m are the missile position coordinates and $\hat{x}_{ij}$ and $\hat{z}_{ij}$ are the guessed target position coordinates corresponding to the range guess $\hat{R}_{ij}$.

$$\begin{bmatrix}\hat{x}_{ij}\\ \hat{z}_{ij}\end{bmatrix} = \hat{R}_{ij}\begin{bmatrix}\cos\lambda\\ \sin\lambda\end{bmatrix} + \begin{bmatrix}x_m\\ z_m\end{bmatrix} \tag{3.2}$$

Therefore, for every $\left(\hat{V}_{t_i}, \hat{\gamma}_{t_j}\right)$ guess couple, there is a unique target position. That means, one can divide the search space into pieces of speed and angle guesses and find the corresponding guessed target position. That correspondence can be called as *guessed position matrix* (GPM), which is actually the grid created within the preselected search space. A visual representation of GPM can be observed in Figure 3.2.

$$\begin{array}{c|cccc} & \hat{\gamma}_{t_1} & \hat{\gamma}_{t_2} & & \hat{\gamma}_{t_J} \\ \hat{V}_{t_1} \longrightarrow & (\hat{x}_t, \hat{z}_t)_{11} & (\hat{x}_t, \hat{z}_t)_{12} & \cdots\cdots & (\hat{x}_t, \hat{z}_t)_{1J} \\ \hat{V}_{t_2} \longrightarrow & (\hat{x}_t, \hat{z}_t)_{21} & & & \\ & & \vdots & & \vdots \\ \hat{V}_{t_I} \longrightarrow & (\hat{x}_t, \hat{z}_t)_{I1} & & \cdots\cdots & (\hat{x}_t, \hat{z}_t)_{IJ} \end{array}$$

Figure 3.2. Guessed Position Matrix

If the possible guessed speed range of the target is divided into I pieces and the angle range is divided into J pieces; that means there are $J \times I = N$ number of elements in the search space.

3.2.2. Synthetic Trajectories

Assuming that the guess couples are fine enough (small grids), one of the elements in the search space must be the real case. That is, one guess couple should match the real one if the target does not accelerate. The problem now, is to isolate the real couple from the others. One way of doing so, is to create so-called *synthetic trajectories* using the GPM.

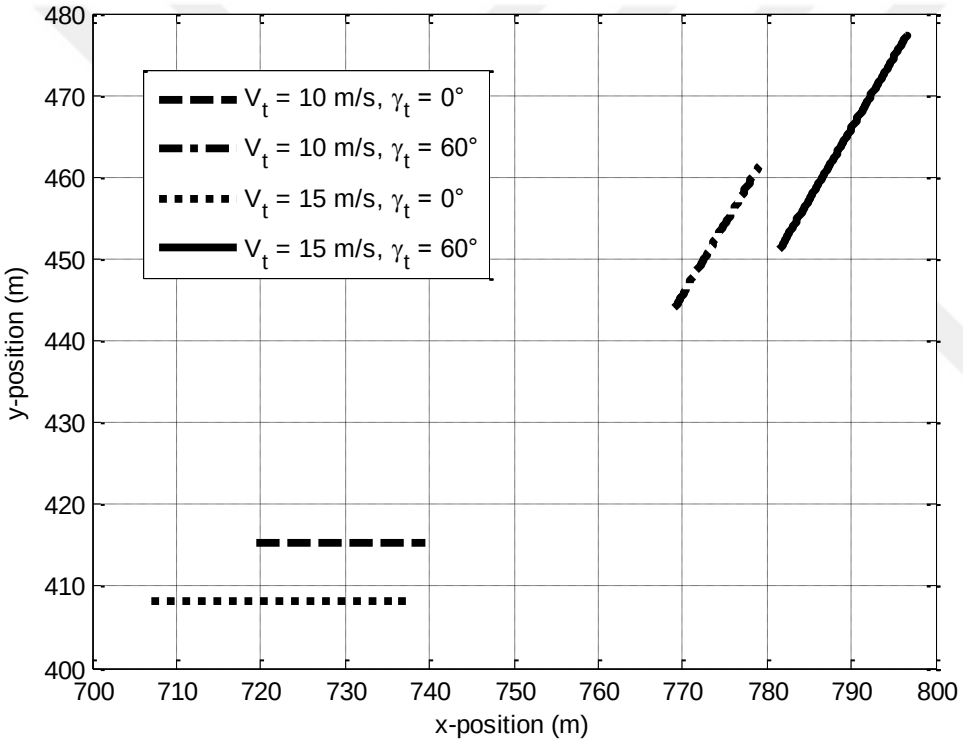

Figure 3.3. Sample synthetic trajectories for 2 seconds

Suppose that, in a certain time step, the abovementioned calculations are made and the GPM is constructed. Each target position guess in the GPM has their own unique velocity vector. By exploiting that fact, that position can be integrated and a unique trajectory, of which authenticity should be checked, can be calculated. Performing the

same operation for every element of the GPM results in N number of *synthetic* trajectories.

3.2.2.1. Sample Synthetic Trajectory Calculation[1]

For clarity, the calculations described so far are explained with a numerical example. Suppose a missile has a speed of 300 m/s and it is flying straight ($\gamma_m = 0°$), initially starting from origin. Moreover, the seeker of the missile provides the LOS angle as $\lambda = 30°$ and the LOS angular rate as $\dot{\lambda} = 10°/s$ at a specific timestep.

The guess couples are decided as follows:

- $\hat{V}_{t_1} = 10$ m/s, $\hat{V}_{t_2} = 15$ m/s
- $\hat{\gamma}_{t_1} = 0°$, $\hat{\gamma}_{t_2} = 60°$

Using (3.1), the GPM can be constructed as in Table 3.1.

The position values in the GPM would be used as the initial conditions for their respective synthetic trajectories. Those trajectories would be integrated by using their own speed and angle values, creating four distinctive flight paths for four different virtual targets.

Table 3.1. GPM for sample calculation

	$\widehat{\boldsymbol{\gamma}}_{\boldsymbol{t_1}} = \mathbf{0}$	$\widehat{\boldsymbol{\gamma}}_{\boldsymbol{t_1}} = \mathbf{60}$
$\widehat{\boldsymbol{V}}_{\boldsymbol{t_1}} = \mathbf{10}$	$[719.5, 415.4]\ m$	$[769.1, 444.0]\ m$
$\widehat{\boldsymbol{V}}_{\boldsymbol{t_2}} = \mathbf{15}$	$[707.1, 408.2]\ m$	$[781.5, 451.4]\ m$

For the sake of illustration, those trajectories are integrated for two seconds and plotted in Figure 3.3 (note that the missile trajectory is not plotted here for simplicity). Here, the lack of uniqueness of trajectories can easily be seen. Not only their initial conditions are different; but also, they follow very different paths (although parallel). The algorithm would exploit that fact and use it as a tool to isolate the real case from the others.

[1] At this point, the aim is not to estimate something; but to create the synthetic trajectories *only*

3.3.Isolation of the Correct Case within Search Space

So far, the working domain of the algorithm was established by using physical limitations. After establishing the search space domain, the task evolves to *searching* for the true case.

3.3.1. Synthetic LOS/LOS Rate Profiles

The synthetic trajectories are the focus of the isolation algorithm as one of the trajectories should match the true engagement. Therefore, a property of those trajectories must be used to compare with the real measurements. For that end, by assuming constant target velocity, as the synthetic trajectories are integrated, each trajectory would produce its own LOS and LOS rate profiles, called *synthetic LOS (rate) profiles*. Then, one can compare those synthetic profiles with the real measurement, by defining a cost function, to isolate the true case.

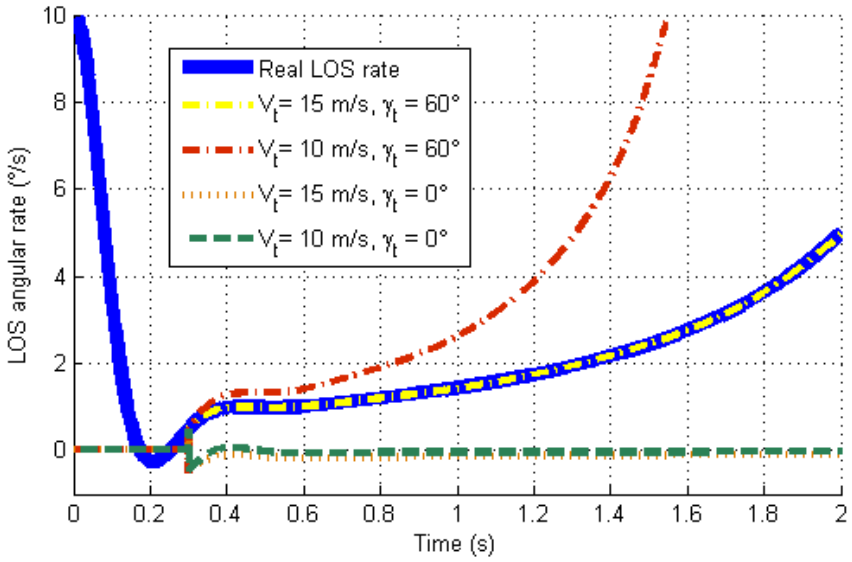

Figure 3.4. Resultant synthetic and real LOS rate profiles for the sample scenario

To illustrate, the example GPM depicted in Table 3.1 is used for further analysis in order to create the synthetic LOS rate profiles by adding a real target to estimate. This time, the real target is assumed to be flying with 15 m/s and an angle of 60° (which happens to be exactly the same as one of the elements in the GPM). The resultant LOS

rate profiles of the synthetic trajectories and the real LOS rate are presented in Figure 3.4, where all measurements are assumed to be ideal.

In this sample, the algorithm is initiated at 0.3 seconds at which the GPM is created. Then, the sample synthetic trajectories are constructed (Figure 3.3). For each trajectory, since the corresponding guessed target position (hence, the range) and velocity are known, using (3.3), derived from (2.2), synthetic LOS rate profiles depicted in Figure 3.4 can be constructed.

$$\hat{\dot{\lambda}}_{ij} = \frac{V_m \sin(\hat{\lambda}_{ij} - \gamma_m) - \hat{V}_{t_i} \sin(\hat{\lambda}_{ij} - \hat{\gamma}_{t_j})}{R_{ij}} \tag{3.3}$$

$\hat{\lambda}_{ij}$ indicates the guessed LOS angle (*synthetic LOS angle*), corresponding to i^{th} guess of speed and j^{th} guess of target flight path angle, calculated by simply taking the arctangent of the synthetic target position and true missile position.

Inspection of Figure 3.4 suggests the successful capture of the real trajectory. The LOS rate profiles of both the synthetic (yellow-dash dotted) and the real (thick blue) profiles are exactly the same. The exact similarity could be obtained due to the facts that:

1) Measurements are ideal
2) The real case exactly matches to the initial guess in the GPM

3.3.2. Comparison via Cost Function

After obtaining the synthetic LOS rate profiles (or LOS profiles), the problem becomes to finding a metric to isolate the real case from others.

The proposed methodology for the isolation is to calculate the difference between the measured LOS rate (or LOS) and the synthetic LOS rates (or LOS), which from this point on would be called as *errors*. Those errors would be accumulated within an integral (a cost function), shaped as desired. One can immediately infer that, instantaneously calculating the errors are enough to distinguish the actual case from the others. However, as previously stated, the given sample is ideal and in a non-ideal world the measurements would deviate from what they should be; making error accumulation in an integral a must.

Nevertheless, as long as the target moves without acceleration, even if there are errors in measurements, on the long run, the LOS and LOS rate profiles other than the real case should move away from the real case. Therefore, rather than looking for errors at every instant separately, the summation of errors should be a better solution. If LOS rate is taken as the main source of comparison, it can be used as an error source by taking the integral of the error (3.4).

$$e_{\lambda}^{ij} = \int_{t_i}^{t_f} \left| \dot{\lambda}_{meas} - \hat{\dot{\lambda}}_{ij} \right| dt \tag{3.4}$$

The main purpose of this equation, is to collect the errors by summing their absolute values within a period of time. By doing so, LOS rate profiles obtained from unrelated synthetic trajectories would deviate from the real profile, rendering the integral larger, making the distinguish of the real case easier.

Nevertheless, (3.4) can be diversified by different means. For example, instead of using absolute values, one can take the square. of the errors, as in (3.5).

$$e_{\lambda}^{ij} = \int_{t_i}^{t_f} \left(\dot{\lambda}_{meas} - \hat{\dot{\lambda}}_{ij} \right)^2 dt \tag{3.5}$$

Similarly, one can choose to compare LOS angles, rather than LOS angular rates. The corresponding LOS angles can be calculated using (3.6), where z_m and x_m are the missile position coordinates.

$$\hat{\lambda}_{ij} = atan2\left(\hat{z}_{ij} - z_m, \hat{x}_{ij} - x_m\right) \tag{3.6}$$

Like in (3.4), the errors can be calculated as in (3.7).

$$e_{\lambda}^{ij} = \int_{t_i}^{t_f} \left| \lambda_{meas} - \hat{\lambda}_{ij} \right| dt \tag{3.7}$$

The hypothesis is that, whichever guess couple minimizes the error value (e_{λ}^{ij}, $e_{\dot{\lambda}}^{ij}$ or any combination of those) should correspond to the real case.

To illustrate that, the integral values of the errors in the example are presented in Table 3.2, in which the errors are calculated by using absolute value method. For this example, the integration is started at $t_i = 0.3$ seconds and finished at $t_f = 2$ seconds.

Therefore, it can be concluded that, the estimated target can be selected as $\hat{V}_t = 15$ m/s and $\hat{\gamma}_t = 60°$ by looking at the minimum of the errors; which resulted in zero, since all measurements are perfect and the target scenario exactly matches with one of the previously determined guess couple.

Table 3.2. Cost functions corresponding to each guess couple in sample scenario

$\hat{V}_{t_i}$ (m/s)	$\hat{\gamma}_{t_j}$ (°)	e_{λ}^{ij} (rad.s)	$e_{\dot{\lambda}}^{ij}$ (rad)
15	60	0	0
10	60	0.06393	0.3457
15	0	5.373	0.06386
10	0	5.376	0.06106

To sum up, the workflow of the algorithm would consist of the following steps:

- In a single timestep, the GPM is created.
- Using the elements of GPM as initial conditions, synthetic trajectories are created.
- Each synthetic trajectory would result in its own LOS and LOS rate profiles (*synthetic LOS profiles*).
- At each time step, the measured LOS and LOS rates are compared with their respective synthetic LOS and/or LOS rate profiles.
- Finally, the synthetic LOS and/or LOS rate profile that is closest to the measurements belongs to the real engagement.

Moreover, the isolation can be augmented by different means. Namely, some element in GPM could be ignored, as they may give unrealistic results. Assume that the algorithm would be implemented to a missile, having the following characteristics:

- Maximum range: 10 km
- Maximum altitude: 5 km

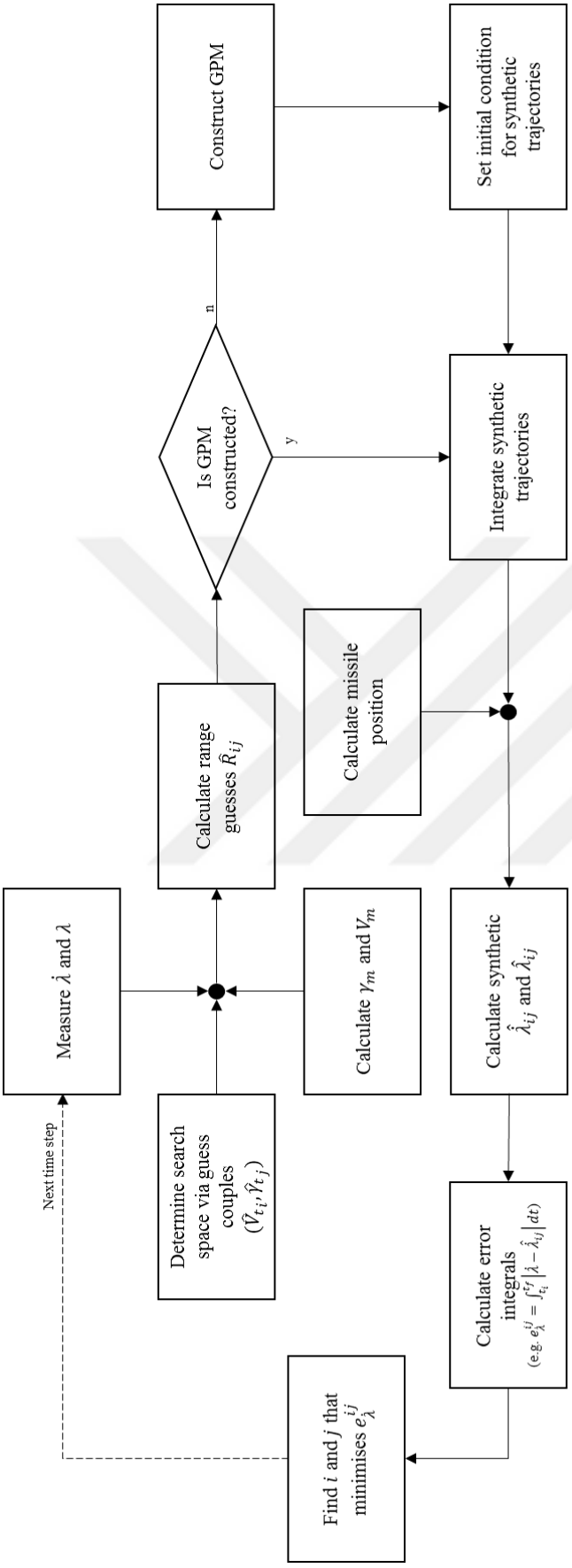

Figure 3.5. Algorithm workflow

By using this knowledge, one can choose to disregard the elements in GPM, which provides a synthetic range larger than 10 km and smaller than 0 km (as it would be meaningless to have negative range). Similarly, the elements which has a z-position larger than 5 km can also be ignored as the designer may assert that estimating a target beyond the capabilities of the missile would be meaningless.

This phenomenon is further explained in the last chapter under *Future Work*.

3.4.Sensitivity of Range Estimation to Guess Couple Selection

The sample scenario given previously assumed that the real target velocity exactly matched with one of the guess couples. This mostly would not be the case in real scenarios. However, if the grid of the guess couples are constructed fine enough, the resultant estimation could be within the vicinity of the real scenario, making a close estimation possible. So, the question becomes: "The physical limits in question should be partitioned into how many grids?".

There is a trade-off between computational effort (analysed in Chapter 5) and estimation performance. The finer the search grid (the more elements the GPM has), the better the estimation performance. However, since there would be too many elements in the GPM, resulting in too many integrations and consequently, too much computational time. Therefore, the grid partitioning should be optimised.

The methodology to be followed is to look at how the calculations are affected if the real target velocity does not match with a guess couple. To do so, the real speed and angle values are perturbed from their original values as shown in (3.8) and (3.9). Their effects to range calculation are analysed as the range estimation is important to the algorithm since it is the initial condition for each guess. Note that in (3.8) and (3.9), the subscripts of i and j are dropped from $\hat{\gamma}_t$ and $\hat{V}_t$ for clarity.

$$\hat{\gamma}_t = \gamma_t + \Delta\gamma_t \tag{3.8}$$

$$\hat{V}_t = V_t + \Delta V_t \tag{3.9}$$

Then, (3.8) and (3.9) are inserted into (3.1), creating a small disturbance ΔR in range.

$$R + \Delta R = \frac{V_m \sin(\lambda-\gamma_m)-(V_t+\Delta V_t)\sin(\lambda-\gamma_t-\Delta\gamma_t)}{\dot{\lambda}} \tag{3.10}$$

Using the trigonometric identity $\sin(x-y) = \sin(x)\cos(y) - \sin(y)\cos(x)$, (3.11) is obtained.

$$R + \Delta R = \frac{V_m \sin(\lambda-\gamma_m)-(V_t+\Delta V_t)(\sin(\lambda-\gamma_t)\cos(\Delta\gamma_t)-\sin(\Delta\gamma_t)\cos(\lambda-\gamma_t))}{\dot{\lambda}} \tag{3.11}$$

Assuming small angle assumption where $\sin(\Delta\gamma_t) \approx \Delta\gamma_t$ and $\cos(\Delta\gamma_t) \approx 1$, (3.12) is found.

$$R + \Delta R = \frac{V_m \sin(\lambda-\gamma_m)-(V_t+\Delta V_t)(\sin(\lambda-\gamma_t)-\Delta\gamma_t\cos(\lambda-\gamma_t))}{\dot{\lambda}} \tag{3.12}$$

Rearranging gives (3.13).

$$R + \Delta R = \frac{\overbrace{V_m \sin(\lambda-\gamma_m)-V_t\sin(\lambda-\gamma_t)}^{R}}{\dot{\lambda}} - \frac{(V_t\Delta\gamma_t\cos(\lambda-\gamma_t))-(\Delta V_t\sin(\lambda-\gamma_t))+(\Delta V_t\Delta\gamma_t\cos(\lambda-\gamma_t))}{\dot{\lambda}} \tag{3.13}$$

Finally, the effect of the perturbations is available in (3.14).

$$\Delta R = -\frac{V_t\cos(\lambda-\gamma_t)}{\dot{\lambda}}\Delta\gamma_t + \frac{\sin(\lambda-\gamma_t)}{\dot{\lambda}}\Delta V_t - \frac{\cos(\lambda-\gamma_t)}{\dot{\lambda}}\Delta V_t\Delta\gamma_t \tag{3.14}$$

The immediate assessment of (3.14) clearly indicates that, all deviations in guesses are inversely proportional to the LOS rate. In other words, the agile the engagement (rendering $\dot{\lambda}$ large), the lower the deviations. Besides, since LOS rate is present in every term and it is in the denominator, its effect to each term is the same. Therefore, while comparing the terms, only nominators are taken into account.

If the target is stationary, the deviations in γ_t becomes irrelevant (note that $\Delta\gamma_t$ is multiplied with V_t, which is zero for a stationary target). This makes sense because of the fact that flight path angle for a stationary vehicle is meaningless. The second and third term are rather ambiguous. It includes the expression $\lambda - \gamma_t$ in sine and cosine terms. Since the third term includes $\Delta\gamma_t$ term, it can be assumed that the algorithm cannot estimate γ_t wrong, as all γ_t's are true for all targets, yielding the third term also irrelevant. Still, a mathematical and physical expression for γ_t is unavailable when the target is stationary, making the analysis of the second term hard.

Nevertheless, it can be assumed that since the sine term can have maximum value of 1, it can be assumed that the maximum range error due to velocity estimation error is $\Delta R = \Delta V_t/\dot{\lambda}$.

On the other hand, (noting that the trigonometric functions can only attain a maximum value of 1) if the target is fast (V_t is large) – which could be the case – deviations due to $\Delta\gamma_t$ becomes large; hinting that the $\hat{\gamma}_t$ grids should be as fine as possible.

Likewise, errors due to ΔV_t depends on a trigonometric function, of which maximum is 1. Numerically ΔV_t values are larger than $\Delta\gamma_t$, of which units are m/s and radians, respectively. Therefore, directly comparing the respective terms of the errors are not possible.

To determine the grids, it is selected that, the ratios of the maximum values of the error terms are set equal like in (3.15). While doing that, the last cross-coupling term is disregarded, since it consists of only a trigonometric function and the multiplication of two Δ terms.

$$\left(\frac{V_t\cos(\lambda-\gamma_t)}{\dot{\lambda}}\right)_{max}\Delta\gamma_t = \left(\frac{\sin(\lambda-\gamma_t)}{\dot{\lambda}}\right)_{max}\Delta V_t \tag{3.15}$$

$\dot{\lambda}$ values that maximise the expressions in (3.15) are the same in both sides and maximum values of trigonometric functions are 1. Applying those gives the expression in (3.16).

$$\frac{\Delta\gamma_t}{\Delta V_t} = \frac{1}{V_{t_{max}}} \tag{3.16}$$

(3.16) indicates that the maximum difference between an element of the guess couple and the real values is a function of the maximum possible value of the target. It was mentioned earlier that the $\Delta\gamma_t$ term becomes large when target speed is large, rendering this term dominant in the expression. Therefore, it could be advised that the ratio expressed in (3.16) could be used as the maximum possible value for the grid selection. That is to say, one can choose a finer domain in $\hat{\gamma}_t$ than in $\hat{V}_t$.

To clarify, if the maximum value of a possible target is 500 m/s, when the speed domain is divided with 5 m/s of increments, that means the angle domain should be

divided with 0.01 rad of increments, maximum. Obviously, one can choose to divide the angle domain to smaller increments (e.g. 0.005 rad).

CHAPTER 4

IMPLEMENTATION

4.1.Simulink Environment

The algorithm described above is tested in MATLAB – Simulink environment where the 2D missile – target engagement is simulated. The simulation is run with Euler integration, having a time step of 0.001 seconds.

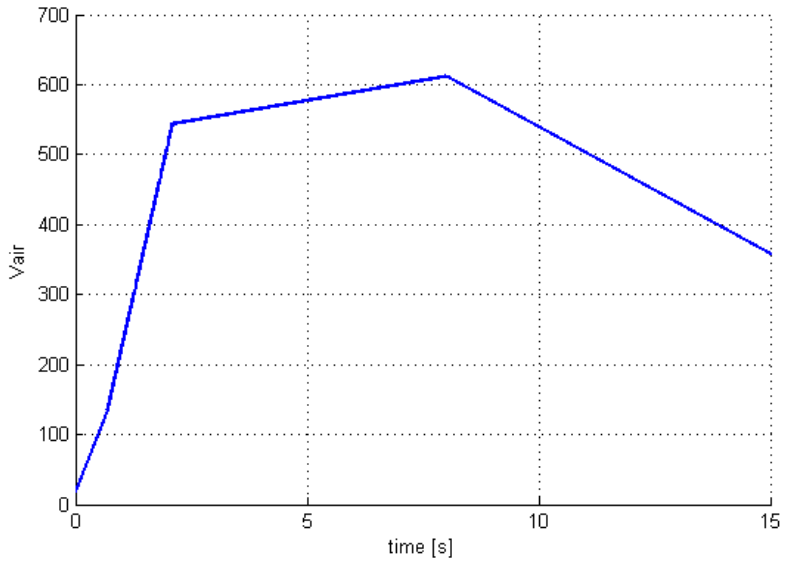

Figure 4.1. Typical speed profile of a missile with boost – sustain – coast sequence

In the simulation, only the kinematics of the target is modelled, as the aerodynamics of the missile is irrelevant since the algorithm only needs good measurements. Nevertheless, the missile is assumed to have a dynamic as described in (4.1).

$$\frac{\gamma_m}{\gamma_{m_{com}}} = \frac{\omega_n^2}{s^2+2\xi\omega_n s+\omega_n^2} \tag{4.1}$$

This transfer function incorporates both the autopilot and guidance dynamics; as well as the CAS dynamics (refer to Figure 2.1). This dynamic is added to the simulation in order to add some realism to the testing environment. Likewise, the missile is assumed to have a typical boost – sustain – coast thrust sequence [27] like in Figure 4.1.

Moreover, the missile is guided to the target via flight path angle guidance law, shown in (4.2) where N is the navigation constant and b is the bias term as depicted in [28].

$$\dot{\gamma}_{m_{com}} = N\dot{\lambda} + b \tag{4.2}$$

A bias term may be added if the algorithm designer would like to avoid the unobservable point where $\dot{\lambda}$ is zero as the bias term may avoid $\dot{\lambda} = 0$ convergence, depending on its value.

For starters, bias value is set to -0.1 rad/s and the navigation constant is set to 3, unless otherwise specified. These parameters are set to their values in order to have good observability even when the target is stationary.

4.2. Real World Effects – Bias & Noise

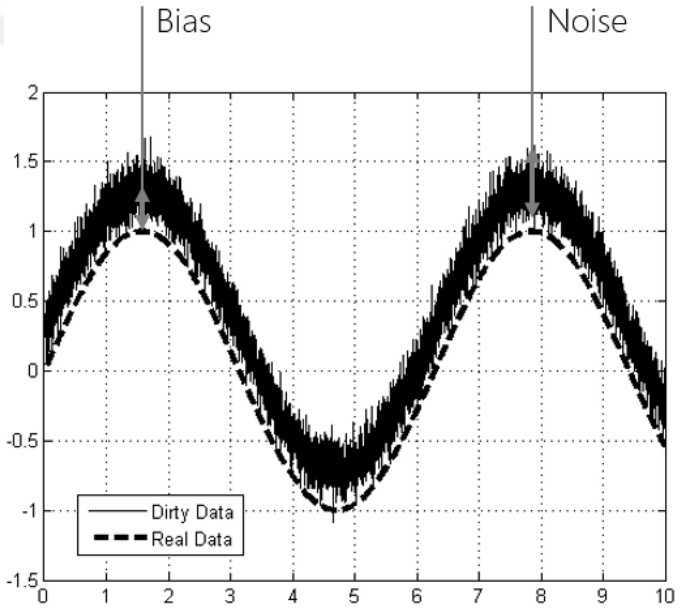

Figure 4.2. Bias and noise in a sample sine wave data

In real applications, the measurements would be either biased or noisy, or both. Noise is called the continuous deviation of the signal from its original value with a mean value of zero. On the other hand, bias is the deviation of the signal from its real value with a non-zero value. To illustrate, in Figure 4.2, the real data (sine wave) is corrupted with a constant bias term (0.3) and a random number generator (variance 0.01).

Bias and noise concepts are also added to the simulation environment to analyse their effects to the performance of the algorithm.

4.2.1. Inertial Measurement Unit Errors

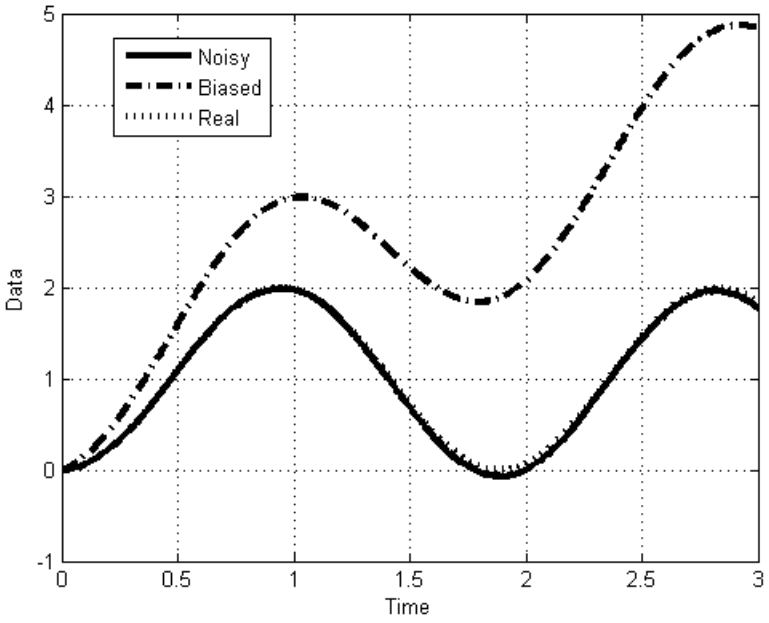

Figure 4.3. Integration of a sine wave signal with noisy (solid) and biased (dash-dotted) data

IMU is the device that measures the acceleration and rotational velocity of the missile body. In order to find the navigational parameters like, speed, position etc. they need to be integrated.

Since noise displays itself around a zero-mean value, its integration does not deviate from the real integral, theoretically. Conversely, since the mean value of the bias is not zero, its integral would accumulate over time. Consequently, as shown in Figure

4.3, while integral of the biased measurement deviates significantly from real values, the integral of the noised measurement does not move away notably. Therefore, it can be asserted that, rather than the noise, bias of the IMU could affect the performance of the algorithm; as it would cause the deviation of the navigational parameters used within the algorithm.

4.2.2.Seeker Errors

A seeker in a missile is mostly mounted on a device called *gimbal*, which rotates the seeker to look at the target directly. As it does so, it rotates around its axes, which creates a rotational velocity. Using this velocity and its current angular position of the gimbal, LOS rate and LOS angle can be constructed [29].

As long as the seeker is locked to the target and the target is kept within the FOV (Field of View), target tracking can be established with negligible bias. However, measurement noise would be present and not negligible. Moreover, most of the IR seekers work with a lower frequency (~50-100 Hz) than the flight computer (~500-1000 Hz) due to image processing algorithms. This means that, there would be less number of real measurement to compare to their synthetic ones; degrading the performance of the algorithm.

It should also be noted that, since the core of the algorithm is based on integrating the absolute value of LOS and/or LOS rate errors between measured and synthetic trajectories. Consequently, any noise in the measurement would accumulate in the error integration.

4.3. Algorithm Customisations Specific to the Thesis

The algorithm to be tested was explained in Chapter 3. It can be asserted that the algorithm has some parameters that may be changed or tuned wherever deemed necessary.

Firstly, the grid of the GPM is selected based on the $1/\hat{V}_{t_{max}}$ rule. A grid of 2.5° is selected for $\hat{\gamma}_t$ along with a selected $\hat{V}_{t_{max}}$ of 400 m/s. This forces a maximum $\Delta\hat{V}_t$ via (4.3) derived from (3.16).

$$\Delta\hat{V}_t = \left(2.5° \times \frac{\pi}{180°}\right)(400\ m/s) = 17.45\ m/s \quad (4.3)$$

For both safety and clarity purposes, the aforementioned speed grid is made finer by setting $\Delta\hat{V}_t = 10$ m/s rather than 17.45 m/s. This means that, there would be a total of $144 \times 41 = 5904$ elements in the GPM

The errors to be integrated are calculated from LOS rate values as in (3.7), rather than LOS errors; unless otherwise is stated. Results for LOS errors are also presented for comparison purposes only, but not for all cases.

The algorithm is initiated at 0.3 seconds, in order to let the missile to gain speed, helping the observability. At 0.3 seconds, the GPM is created and synthetic trajectories are initiated, whereas at 0.5 seconds, integration of LOS/LOS rate errors are started. The reason for this is to let the synthetic trajectories to fall apart for a while such that the error integration would not be affected easily by similar trajectories. Immediately after error integration, the estimations are produced. Nevertheless, one can choose to output estimations after starting integrating errors.

CHAPTER 5

RESULTS AND DISCUSSION

In this chapter, the algorithm displayed in Chapter 3 is tested in the environment described in Chapter 4. This section is divided into two parts. First, some test scenarios are run individually for detailed analysis. While the algorithm is tested with ideal circumstances, the effects of imperfect measurements are also analysed. Further, the effect of guidance parameters is also investigated. In the second part, the result of a large batch run environment is shown.

5.1. Individual Results

Table 5.1. Scenario set #1

#	V_t (m/s)	γ_t (°)	x_{init} (m)	z_{init} (m)
1	200	0	500	500
2	140	20	500	500
3	300	240	1000	1000
4	160	180	500	500
5	0	0	750	250
6	20	320	500	500

For ideal and imperfect measurements analyses, a scenario set of 6 different cases are used, as shown in Table 5.1.

The scenarios are selected in a fashion, such that it would cover:

- All angle quadrants
- A wide range of target speed
- A stationary scenario
- Only the elements in the GPM

5.1.1. Ideal Results

To begin the analysis, firstly, the environment is set to an ideal one. That is, all measurements are perfect and all scenario cases happen to match exactly one of the guess couples. In other words, one of the guessed target velocity is exactly the true target velocity.

The resultant trajectories of the scenarios can be seen in Figure 5.1. Likewise, in Figure 5.2 and Figure 5.3, estimates for speed and angle can be seen, respectively.

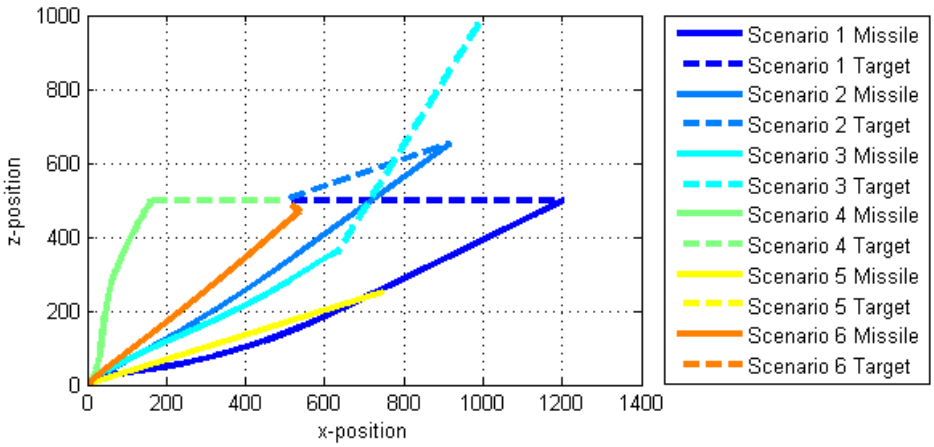

Figure 5.1. Resultant trajectories for ideal case

Figure 5.2, Figure 5.3 and Figure 5.4 clearly indicate that the algorithm can estimate the target velocity, as well as the range. As all the measurement are ideal, and the real target velocity exactly matches to one of the elements in the GPM, perfect estimation is acquired.

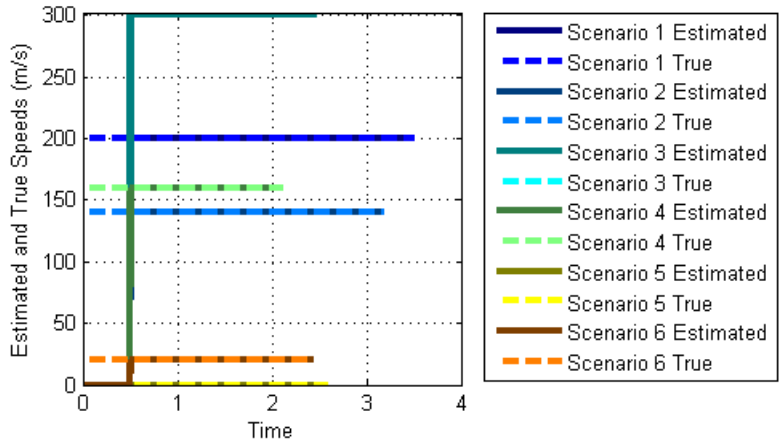

Figure 5.2. Estimated speeds for ideal case

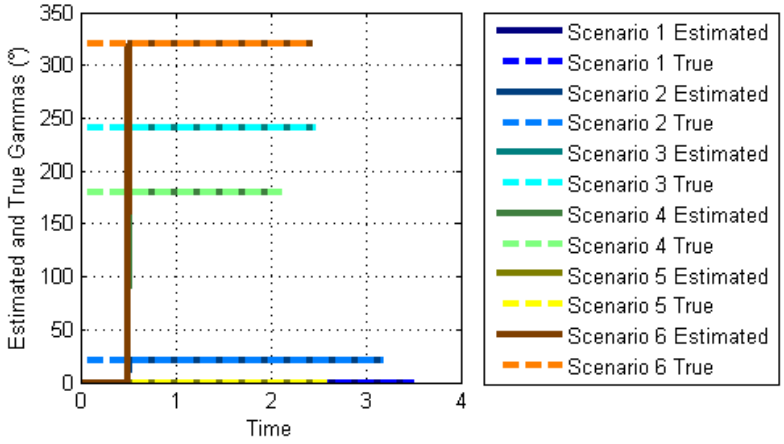

Figure 5.3. Estimated flight path angles for ideal case

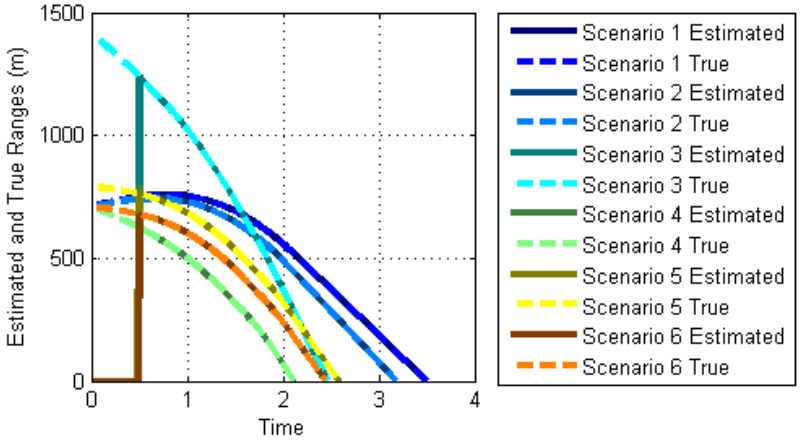

Figure 5.4. Estimated and true ranges for ideal case

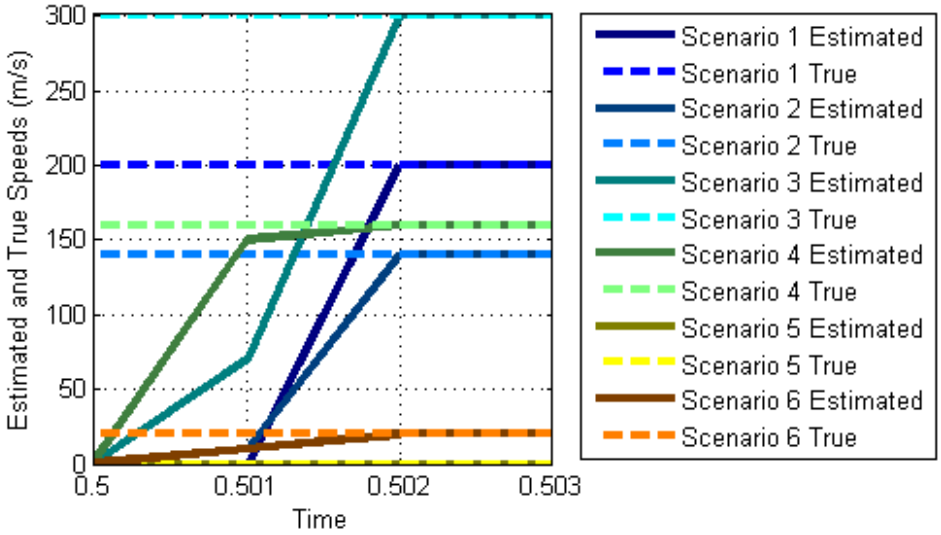

Figure 5.5. Zoomed speed estimations for ideal case when the error integration is started (0.5 s)

However, the uniqueness problem emanates itself even when everything is perfect, as expected. In Figure 5.5 – zoomed version of Figure 5.2 – the estimations just after the error integrations is started is plotted. It can be seen that at time 0.501, the first timestep when the algorithm provides its first results, the estimations at hand are gibberish since the algorithm cannot differentiate the true and other trajectories as there are many "*false true*" trajectories due to the fact that the true trajectories are not unique, *yet*.

Nevertheless, in the next timestep, the algorithm can "lock" itself to the true estimations. In the second timestep, the *false true* trajectories are eliminated by adding their error with their previous errors (which were zero). Owing to this error accumulation, in the second timestep, the real true case is isolated from all *false true* and other wrong trajectories.

In summary, it can be said that, at least two timesteps are required to distinguish the true trajectory from other synthetic trajectories; proving the loss uniqueness in a passive seeker case.

5.1.2. Imperfect Results

The effect of imperfections is handled in four parts. Firstly, the effect of noise and bias of IMU on the algorithm is tested. Then, the seeker is contaminated with errors,

separately from IMU errors. Following that, both IMU and seeker errors are added to the simulation environment. Finally, cases when the target is not an element of the GPM is investigated. While doing so, in measurement error cases, the scenario set shown in Table 5.1 is used. For non-element case, a different scenario set is used, which is presented in its own section (Table 5.3).

5.1.2.1. IMU Errors

In this part, only the IMU noise and bias errors are added to the simulation. The values for noise and bias are based on Honeywell HG1930BA50 IMU of which data is provided in [30]. The results of this case are plotted in Figure 5.6, Figure 5.7 and Figure 5.8.

Similar to the previous ideal case, correct estimation is established despite IMU error. This means that, with previously designated errors in IMU, the synthetic trajectories do not deviate much to change the synthetic LOS rates; making the LOS rate comparison easier.

One difference that can be seen is the range estimates which are calculated using the navigation data, integrated from biased IMU measurements. In Figure 5.8, this difference is imperceptible to the human eye, however, when the integral of the estimation errors are calculated, Figure 5.9 can be obtained. Clearly, the errors in scenario 5 are significantly larger than other scenarios. The reason for this difference lies within the observability problem. Since the target is stationary in Scenario 5, the real LOS rates lie around zero; forcing any errors within the GPM to grow obeying (3.1).

Also, one can notice the jumps at the last phases of the estimation. This can also be explained by the abrupt change in LOS rates at the final phase of the flight. Similar behaviour can be seen when seeker errors are included to the simulation.

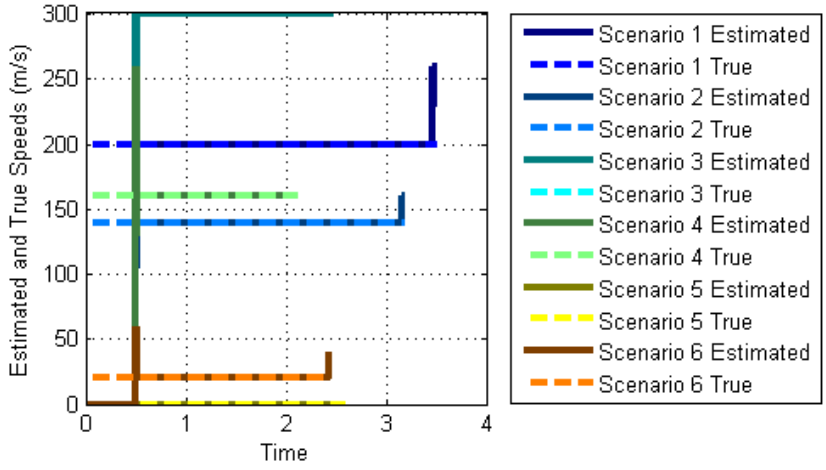

Figure 5.6. Estimated and true speeds for IMU error case

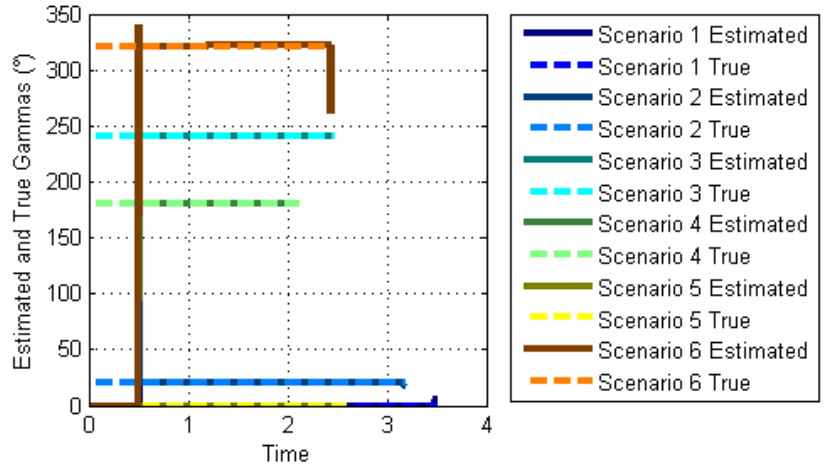

Figure 5.7. Estimated and true flight path angles for IMU error case

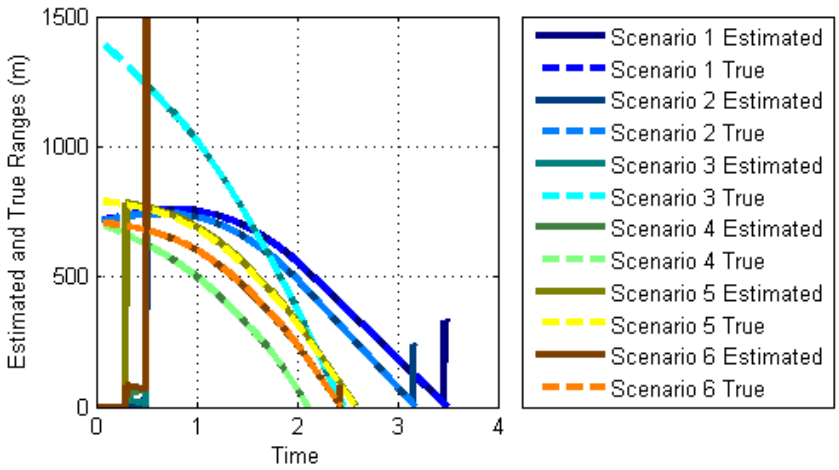

Figure 5.8. Estimated and true range for IMU error case

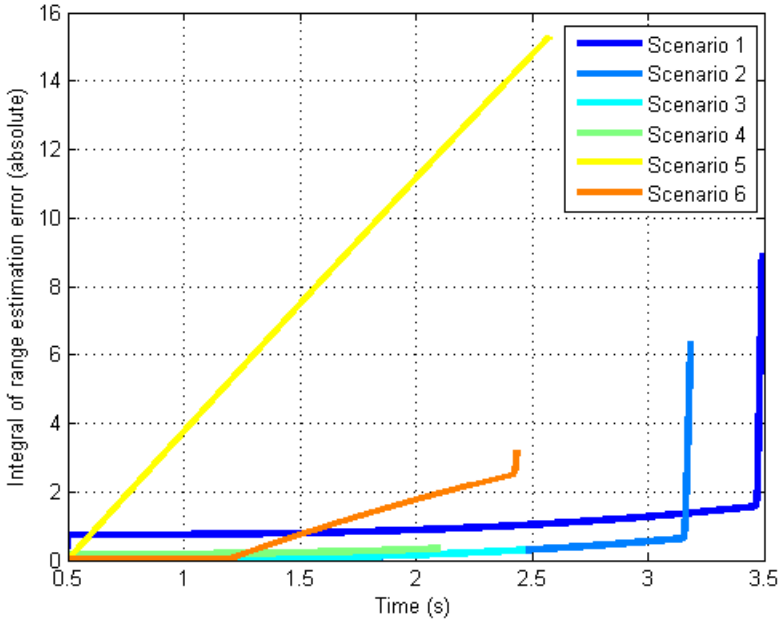

Figure 5.9. Integral of $\left|\hat{R} - R\right|$

5.1.2.2.Seeker Errors

In this section, bias and noise are added to seeker measurements only – errors in IMU are discarded for the time being. It can be said that any errors in seeker measurements could affect the algorithm greatly as they are directly compared to their synthetic counterparts.

It could be considered as hard to find some metrics regarding errors in seeker measurements in literature. An ad hoc approach is adopted using previous experiences in selecting the measurement errors. For that end, bias in measurements are neglected as previously stated; and variances of noise in LOS and LOS rate measurements are selected as 1 mdeg and 0.1 mdeg/s, respectively.

Moreover, the seeker measurements are downsampled to 100 Hz and fed to the algorithm, in order to simulate a more realistic seeker.

The results for this case are provided in Figure 5.10, Figure 5.11 and Figure 5.12.

Immediate assessments of Figure 5.10 and Figure 5.11 shows that, in scenario 5, in which the target is stationary speed estimates are off greatly from their true values (flight path angle estimates are irrelevant as the target is stationary). This can be

explained via (3.14). As the engagement is slow since target in scenario 5 is stationary, the resultant LOS rates at the time when the synthetic trajectories are initiated (0.3 s), attain a very low value (Table 5.2) – closer to zero than other scenarios. Since both LOS and LOS rates are contaminated with noise, any error in both measurements result in a large error in initial synthetic position in GPM calculation. This phenomenon shows that, successful estimation is harder to obtain if the engagement happens slowly.

Nevertheless, when the range estimate of this scenario is investigated, the range estimation seems to be unaffected too much with the failure of the exact estimation of target speed (Figure 5.13). In scenario 5, target speed is zero, meaning that, in (3.14), errors due to $\Delta\gamma_t$ estimations are irrelevant too. Also, target velocity estimation errors are not too much to create large range errors. For this scenario, it can be said that, as the errors are accumulated in the error integral, the algorithm is able to distinguish the real trajectory. Likewise, as the engagement becomes swifter, it is easier for the algorithm to differentiate the real trajectory.

Likewise, when Table 5.2 is observed, the next lowest $\dot{\lambda}$ value at 0.3 seconds after scenarios 5 and 6, is scenario 3. Consequently, observation of Figure 5.12 shows that the next worse estimation performance after scenarios 5 and 6 is scenario 3, correlated with the value of LOS rate. So, it can be inferred that, as the value of $\dot{\lambda}$ increases at the time when GPM is crated, the quality of the estimations also gets better as well; in conjunction with the assessment made in Chapter 3 related to observability.

Table 5.2. LOS rates at 0.3 seconds

Scenario#	**1**	**2**	**3**	**4**	**5**	**6**
$\dot{\lambda}$ **(°/s)**	-9.9588	-4.2464	-3.5308	9.8681	0.0625	-1.5994

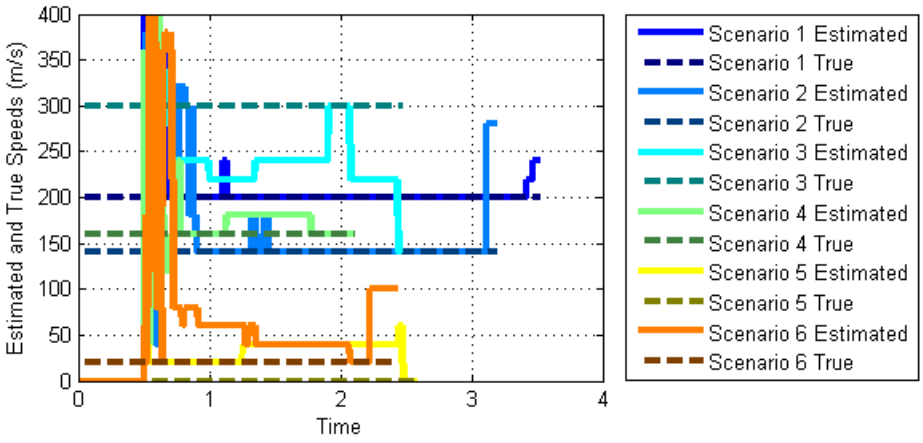

Figure 5.10. Estimated and true speeds for seeker error case

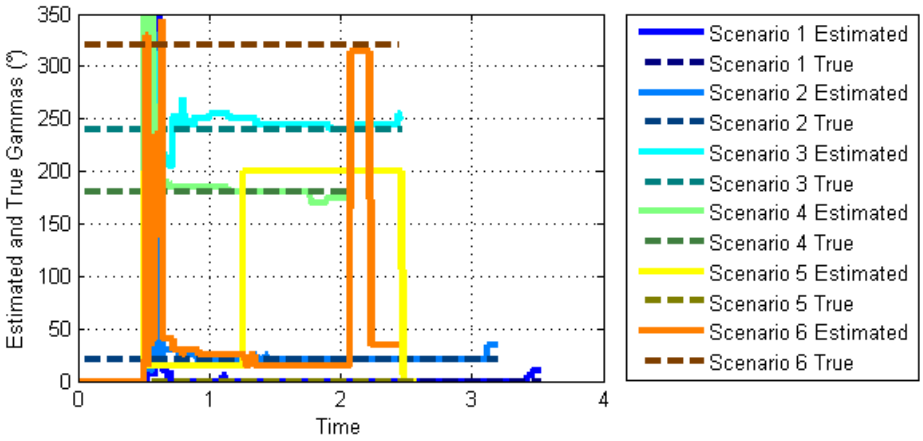

Figure 5.11. Estimated and true flight path angles for seeker error case

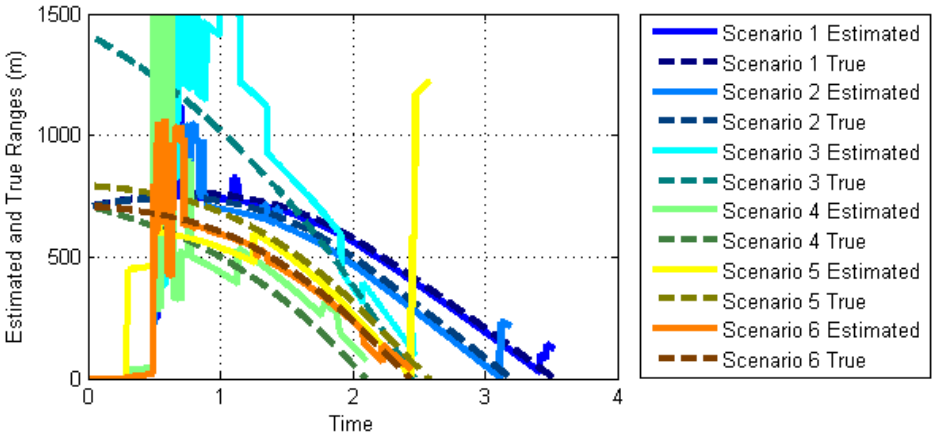

Figure 5.12. Estimated and true ranges for seeker error case

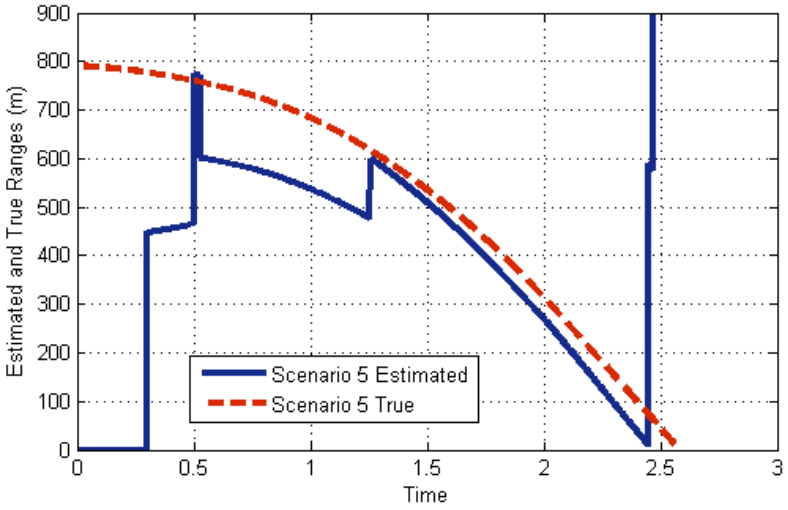

Figure 5.13. Range estimation of scenario 5 for seeker error case

Therefore, the algorithm designer may want to initiate the algorithm not at a specific time, but at a time when the engagement produces relatively large LOS rate values, increasing the chances of obtaining a better GPM.

5.1.2.2.1 Results when LOS Errors are the Error Integration Source

In this part, exactly the same simulation is run, except the source of the integration error, which is taken as in (3.7). The corresponding results are shown in Figure 5.14, Figure 5.15 and Figure 5.16.

Here, with a quick inspection, performance of the algorithm when LOS errors are taken as the source for error integration degrades with respect to the case when integration error source is taken as LOS rate error. Estimation for scenario 6 is completely failed (In Figure 5.16 range estimation of scenario 5 is not within the limits; therefore, it is not plotted for clarity), whereas the performance of other scenarios is worsened.

The reason why the LOS comparison was worse than LOS rate comparison lies within the noise content of those measurements. Generally, noise content of LOS measurements is larger in amplitude than of LOS rate measurements. Therefore, with the analysis performed, it is asserted that, it is better to use LOS rates for error integration. However, one can find a better cost function to minimise that can help selecting the real trajectory.

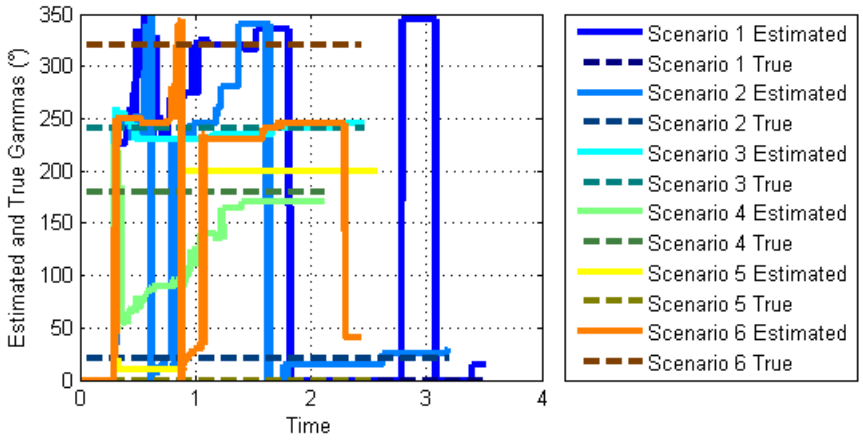

Figure 5.14. Estimated and true flight path for seeker error case with LOS error

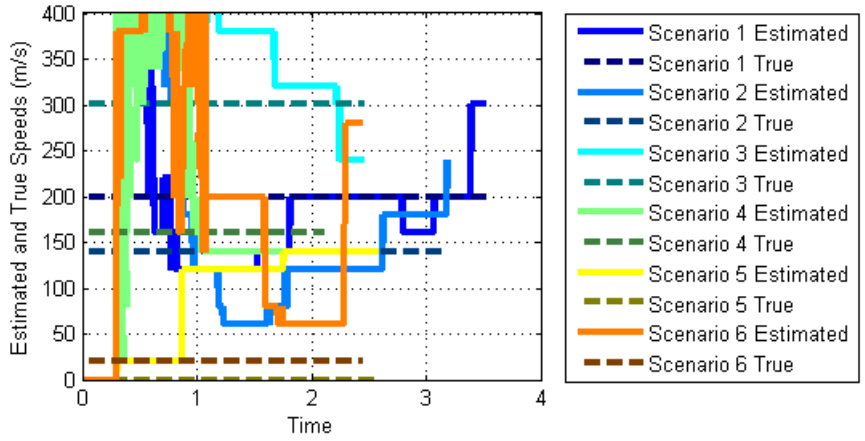

Figure 5.15. Estimated and true speeds for seeker error case with LOS error

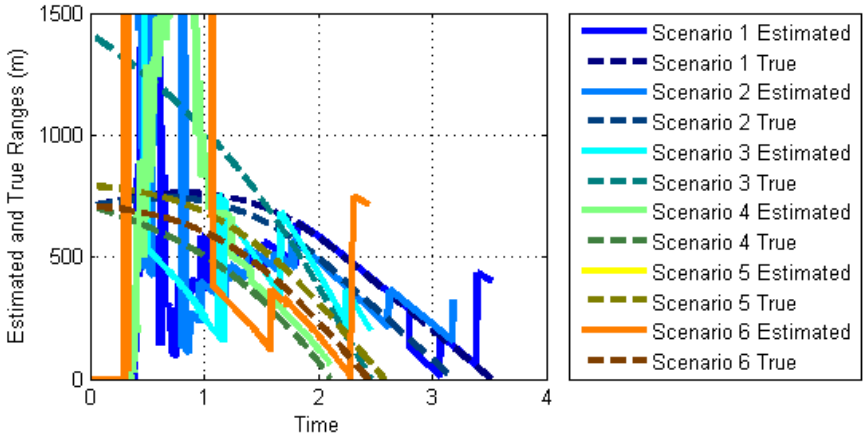

Figure 5.16. Estimated and true ranges for seeker error case with LOS error

It should be noted that, the presented results are a result of the selected measurement error metrics. If one observes a different measurement error in LOS and LOS rate, constructing the cost function via LOS errors may result better results. Nevertheless, with the selected measurement errors in this thesis, cost functions via LOS rate errors provide better results that LOS errors.

5.1.2.3. Combined Errors

In this part, both seeker and IMU errors are added to the simulation. Results are summarized in Figure 5.17, Figure 5.18 and Figure 5.19.

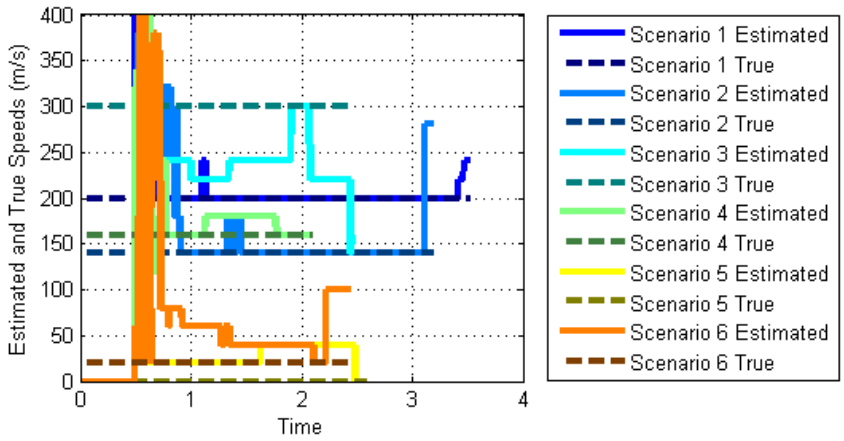

Figure 5.17. Estimated and true speeds for combined error case

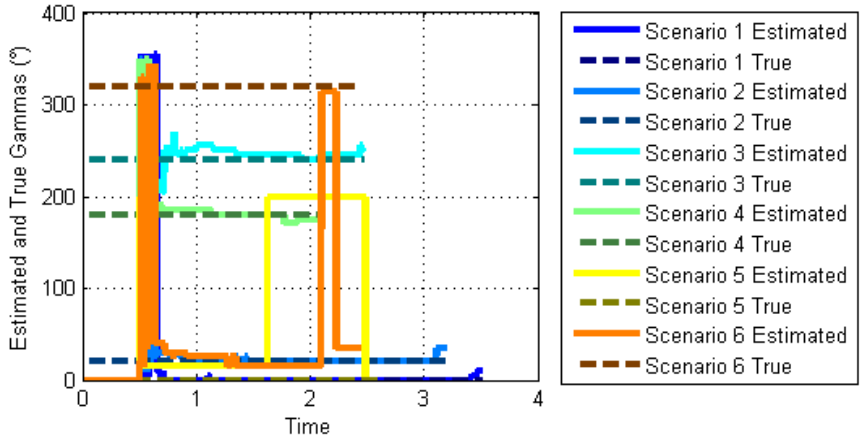

Figure 5.18. Estimated and true target flight path angles for combined error case

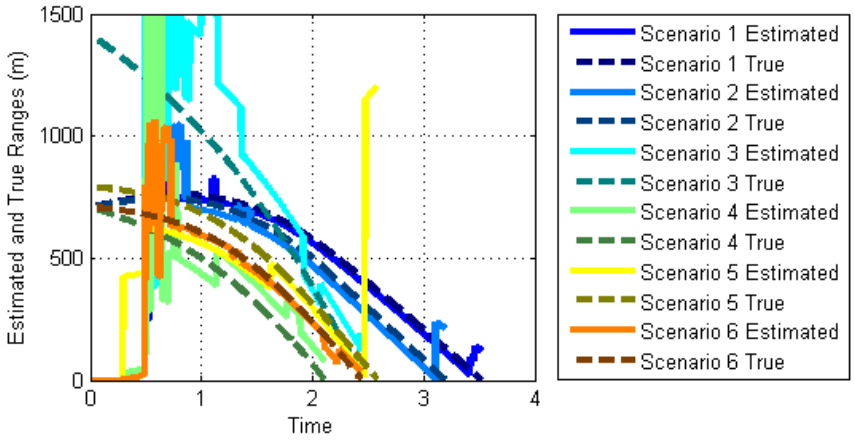

Figure 5.19. Estimated and true ranges for combined error case

As it can be seen from the figures, as expected, errors in IMU did not influence the results much. Consequently, it can be argued that errors in seeker measurements are always dominant in all cases as they are directly compared to their synthetic counterparts.

5.1.2.4. "Non-Element" Case

It is clear that the target velocity vector may not easily match with an element in the GPM. In such a case, it is guaranteed that the initial synthetic position calculation would include some errors forced by (3.14). For that end, 4 sample scenarios are created. Those scenarios and their specifications are summarised in Table 5.3.

Scenarios in Table 5.3 are selected such that, the effects of missing the true target parameters (speed and angle) onto range estimation and how they are affected with the true target speed can be observed. Note that all non-element parameters are selected in such a way that they would lie exactly in the middle of two elements in order to maximise the deprivation effect.

The simulations are run (1) with ideal measurements and (2) with all errors are available. In the following sections, the ideal and non-ideal results are shown; then the corresponding discussion is clarified. In both cases the resultant trajectories are similar and they are plotted in Figure 5.20.

Table 5.3. Scenario set #2

#	V_t (m/s)	γ_t (°)	x_{init} (m)	z_{init} (m)	Notes
1	205	10	3000	50	*High* speed Speed *non-element* Angle *element*
2	200	11.25	3000	50	*High* speed Speed *element* Angle *non-element*
3	20	116.25	1000	50	*Low* speed Speed *element* Angle *non-element*
4	15	115	1000	50	*High* speed Speed *non-element* Angle *element*

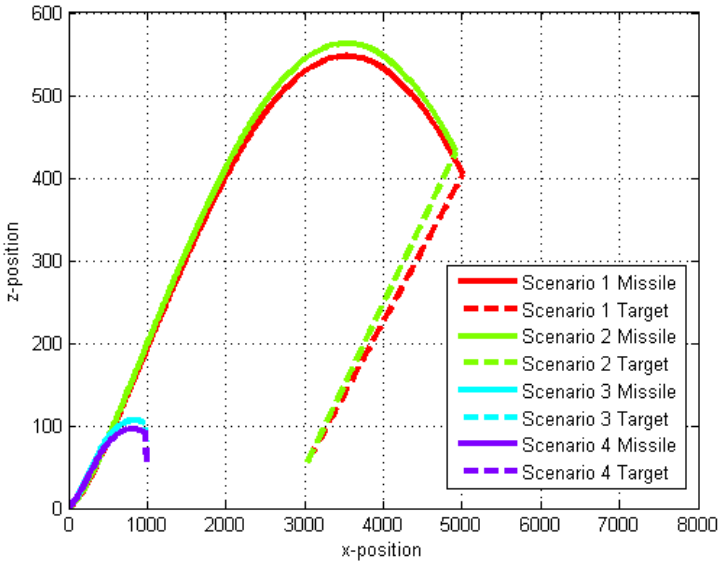

Figure 5.20. Resultant trajectories for scenario set #2

5.1.2.4.1 Ideal Measurements

Results for this case are plotted in Figure 5.21, Figure 5.22 and Figure 5.23.

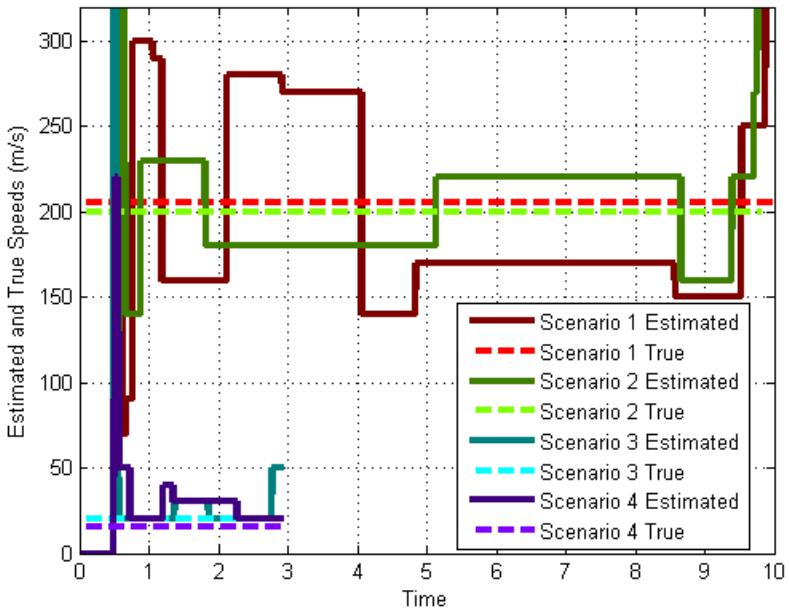

Figure 5.21. Estimated and true speeds for non-element case (ideal)

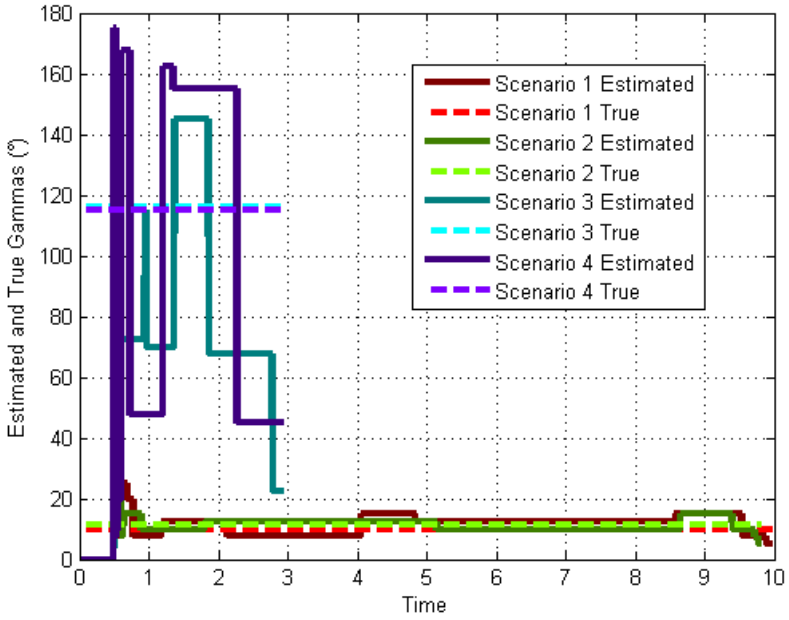

Figure 5.22. Estimated and true flight path angles for non-element case (ideal)

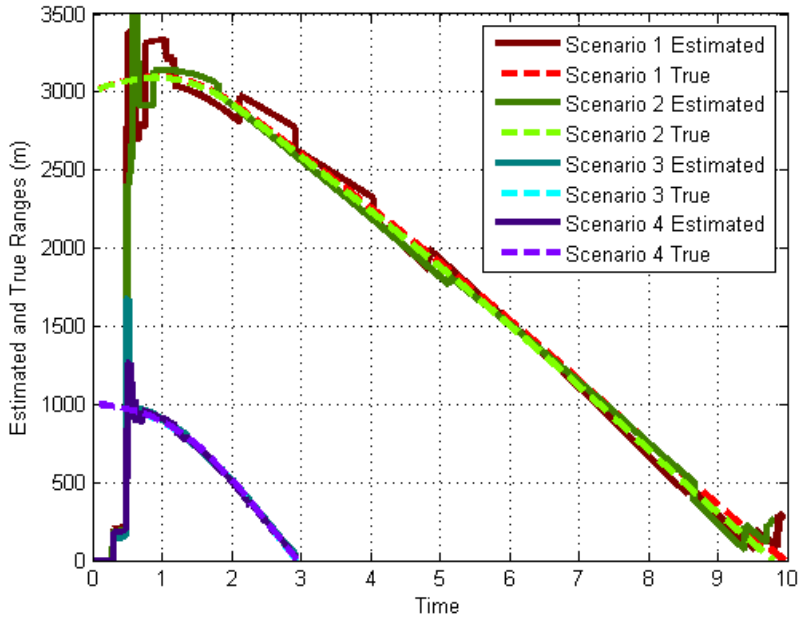

Figure 5.23. Estimated and true ranges for non-element case (ideal)

5.1.2.5. Non-Ideal Measurements

Results for this case are plotted in Figure 5.24, Figure 5.25 and Figure 5.26.

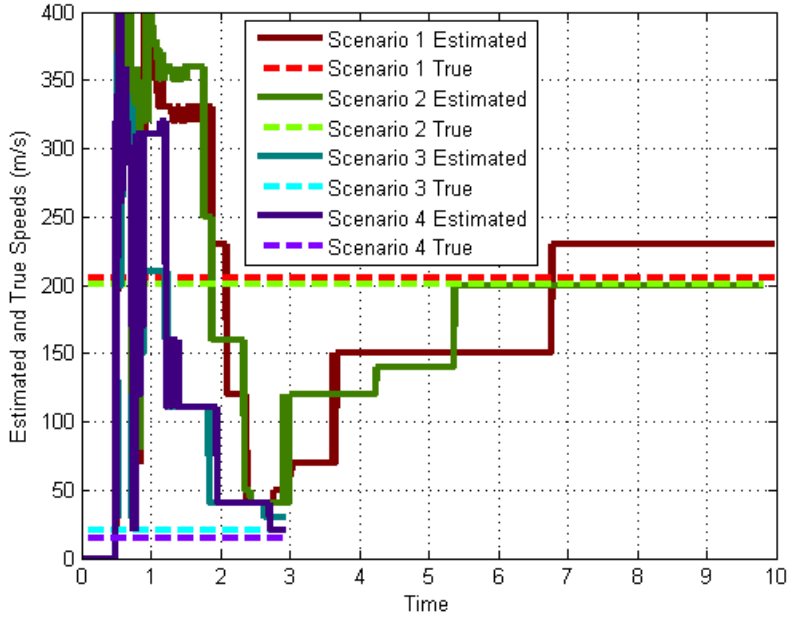

Figure 5.24. Estimated and true speeds for non-element case (non-ideal)

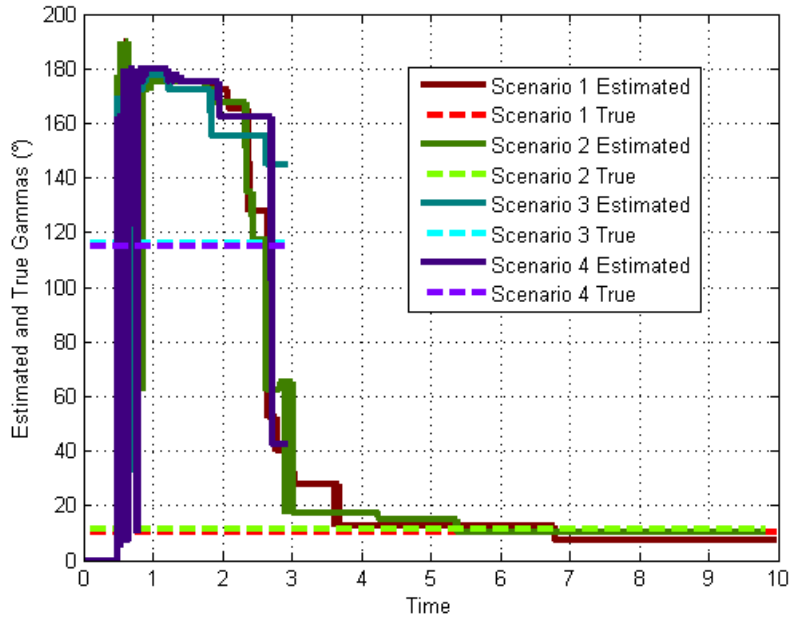

Figure 5.25. Estimated and true flight path angles for non-element case (non-ideal)

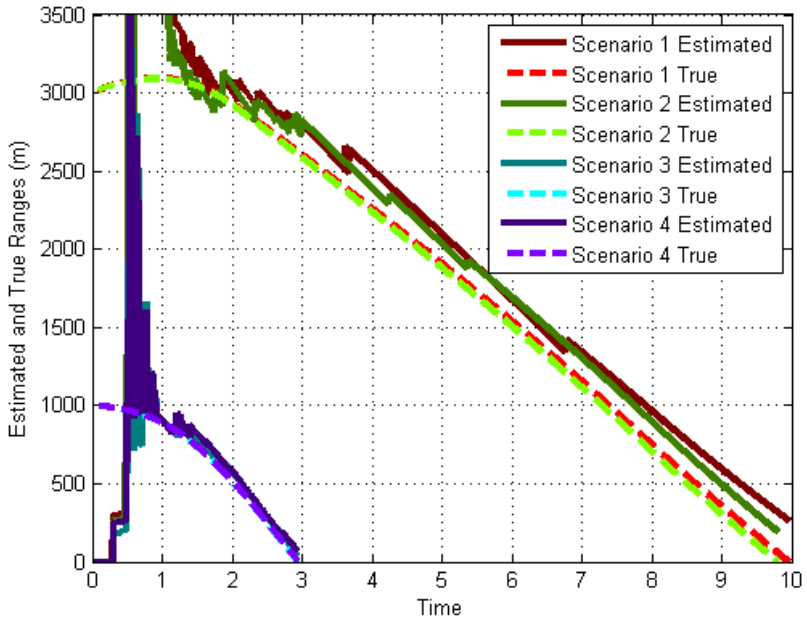

Figure 5.26. Estimated and true ranges for non-element case (non-ideal)

5.1.2.5.1 Discussion of Non-Element Case

One of the quick assessments that can be inferred from the figures plotted above is that, in scenarios 3 and 4, in which the targets are slow, the flight path angle estimates

are considerably off from their true values. Nevertheless, the speed estimates are relatively successful. Consequently, even when the measurements are contaminated with errors, the algorithm is successful in estimating the range. This result can easily be explained by (3.14). When the target is slow, the error term originating from angle estimation becomes smaller than the speed estimation term. Therefore, as long as the target speed estimation is close to its true counterpart (Figure 5.21 and Figure 5.24), a very rough estimation of flight path angle (Figure 5.22 and Figure 5.25) is enough for range estimation for slow targets (Figure 5.23 and Figure 5.26).

Moreover, it can be said that, if the target is slow, it is hard to estimate the flight path angle precisely. This can be explained with the fact that, when the target speed is slow, the synthetic trajectories for the corresponding speed separate very slowly, making the true trajectory harder to be distinguished among false ones. However, as explained above, if the target speed is estimated good enough, a rough estimation of flight path angle is enough to estimate the range.

Another evaluation that can be made is when the target is fast as in scenarios 1 and 2. Again, from (3.14), it can be said that a good flight path estimation is necessary for good range estimation, since now the term with flight path angle error is much more dominant than speed estimation error term. Since the flight path angle is estimated acceptably and speed estimations do not deviate from their true counterparts, the error estimations are close to their true values.

5.1.3.Effect of Guidance Parameters

In this section, the effect of PNG gain and bias to the performance of the algorithm is investigated. To that end, scenario shown in Table 5.4 is used. All cases are run with seeker and IMU errors for better reality.

5.1.3.1.Effect of PNG Gain

Using the scenario conditions in Table 5.4, the analysis is performed under different PNG gains starting from 2 to 8 with an increment of 1, using no bias. The resultant trajectories are plotted in Figure 5.27. As one can predict, as the PNG gain is increased, the missile follows a more agile trajectory, which is expected to have a positive effect to estimation performance.

Table 5.4. PNG gain and bias analysis scenario

#	V_t (m/s)	γ_t (°)	x_{init} (m)	z_{init} (m)
1	200	180	500	500

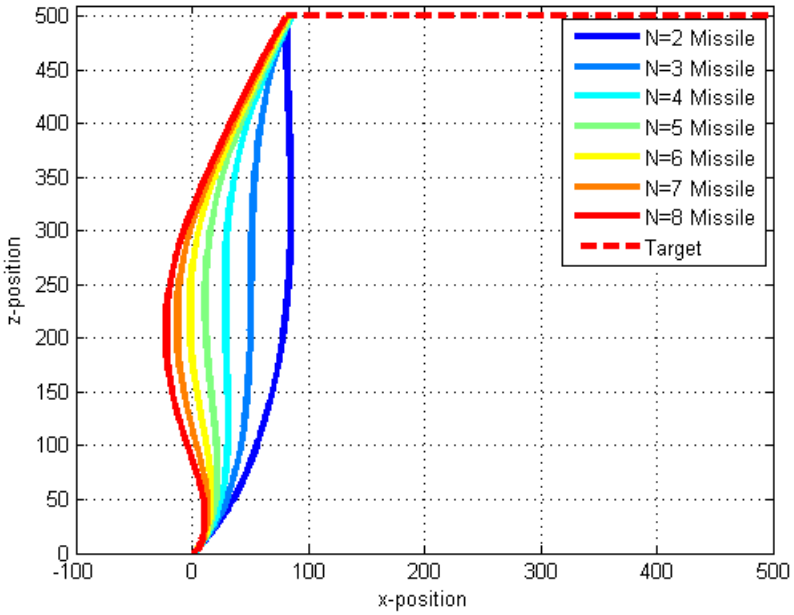

Figure 5.27. Trajectories for PNG gain analysis

The estimated and true parameters are plotted in Figure 5.28, Figure 5.29 and Figure 5.30. In all PNG gain cases, the algorithm captures the true values. However, in each case, the dynamics of the estimation differ from each other. In other words, the time required for the error integral in the algorithm to show the real trajectory is different for each case.

To analyse the effect of PNG gain to the performance of the algorithm, the range estimation performance is used. To that end, the integrals of the absolute error in range is calculated (as in (5.1)) and plotted in Figure 5.31.

$$\Phi = \int_{t_i}^{t_f} \left| \hat{R} - R \right| dt \tag{5.1}$$

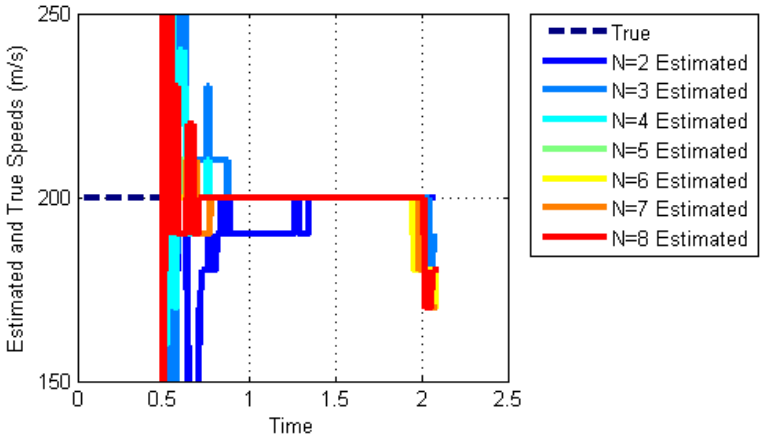

Figure 5.28. Estimated and true speeds for different PNG gains

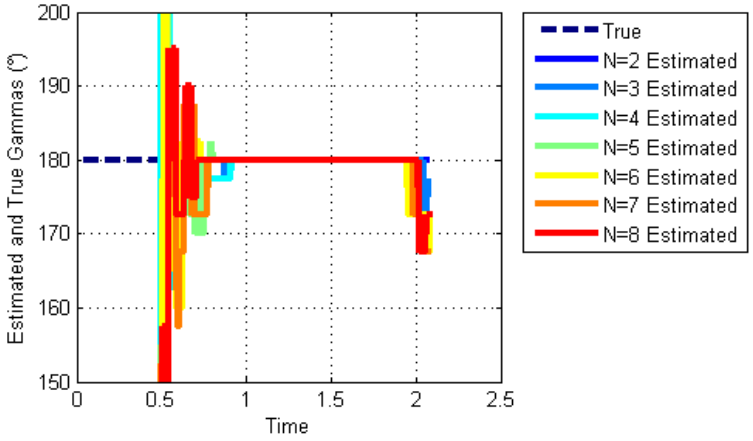

Figure 5.29. Estimated and true flight path angles for different PNG gains

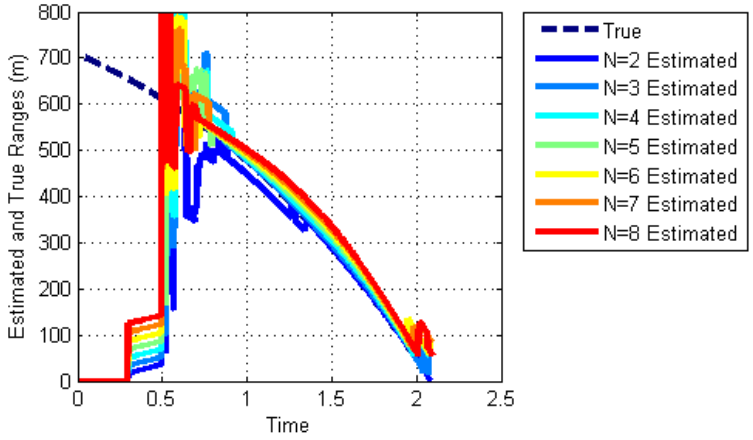

Figure 5.30. Estimated and true ranges for different PNG gains

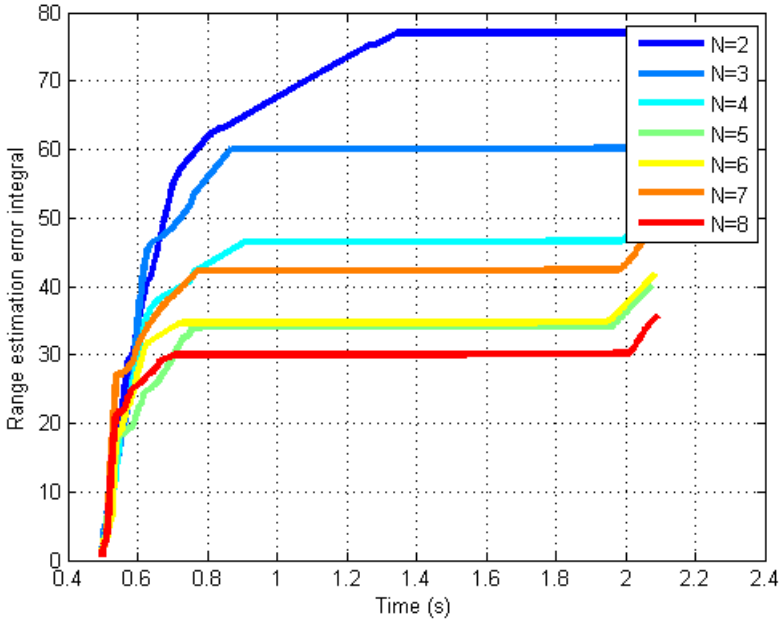

Figure 5.31. Integral of absolute range estimation error for different PNG gains

Figure 5.31 shows the correlation between the PNG gain and the estimation performance. As the PNG gain is increased the estimation performance – although not monotonically – increased owing to the fact that the engagement becomes more agile, helping the observability of the estimation.

5.1.3.2. Effect of Guidance Bias

Similar to the previous section, using the scenario conditions in Table 5.4, the analysis is performed under different guidance bias values starting from -0.3 rad/s to 0.3 rad/s with an increment of 0.1 rad/s, using a PNG gain of 3. Resultant trajectories are plotted in Figure 5.32 which suggests that, as the bias values are increased, missile follows a more aggressive trajectory. This phenomenon, similar to the previous PNG gain analysis, is expected to aid the observability of the system to improve. Related results are plotted in Figure 5.33, Figure 5.34 and Figure 5.35.

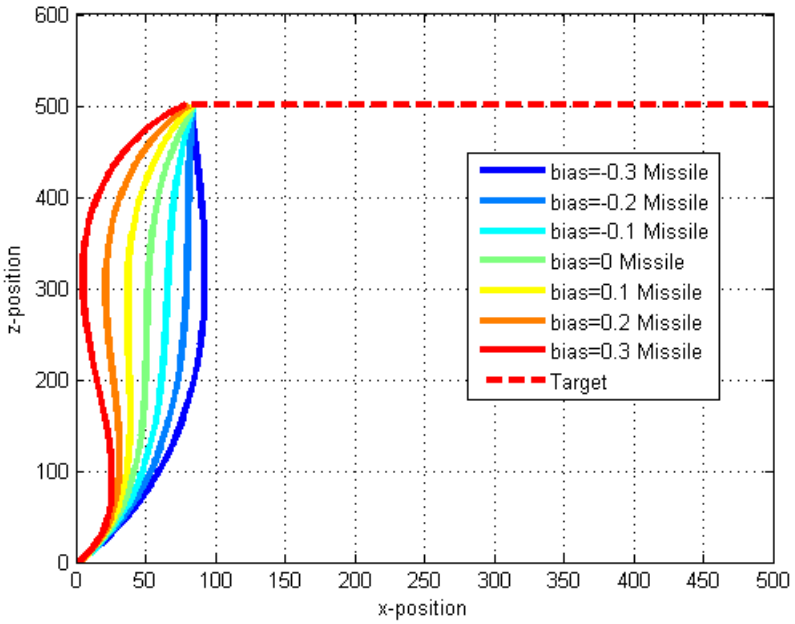

Figure 5.32. Trajectories for guidance bias analysis

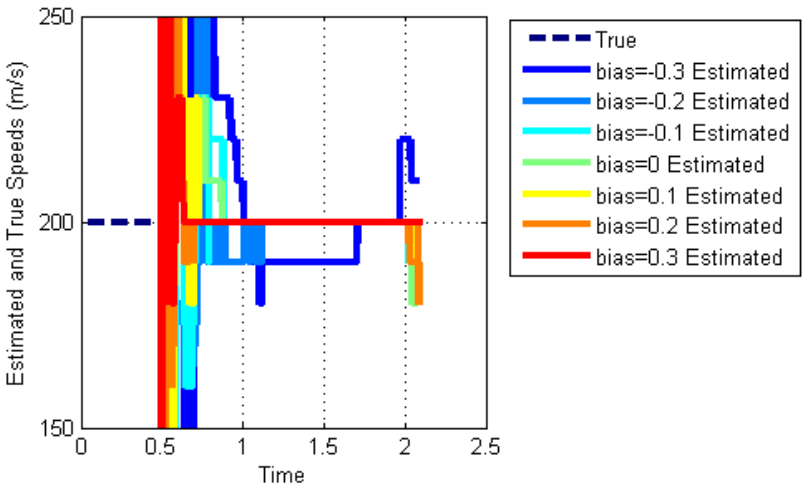

Figure 5.33. Estimated and true speeds for different bias values

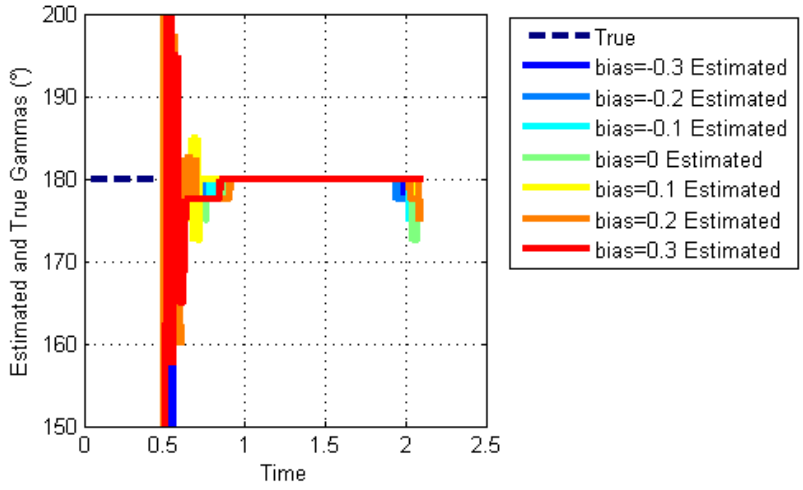

Figure 5.34. Estimated and true flight path angles for different bias values

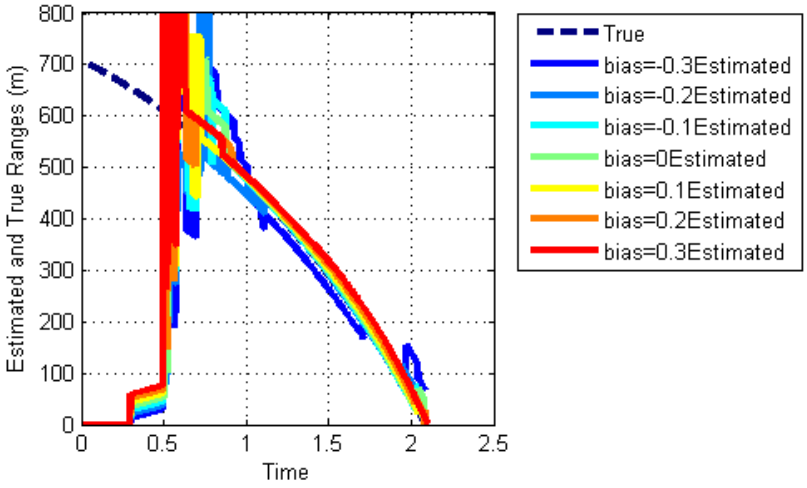

Figure 5.35. Estimated and true ranges for different bias values

Like in the previous PNG gain analysis, in all bias values, the algorithm estimates the parameters successfully, with different transient performance characteristics. To analyse the difference, (5.1) is used and its results are plotted in Figure 5.36 which shows that, in the cases where the bias values making the engagement sluggish, the range estimation performance decreases, in accordance with the previous remark.

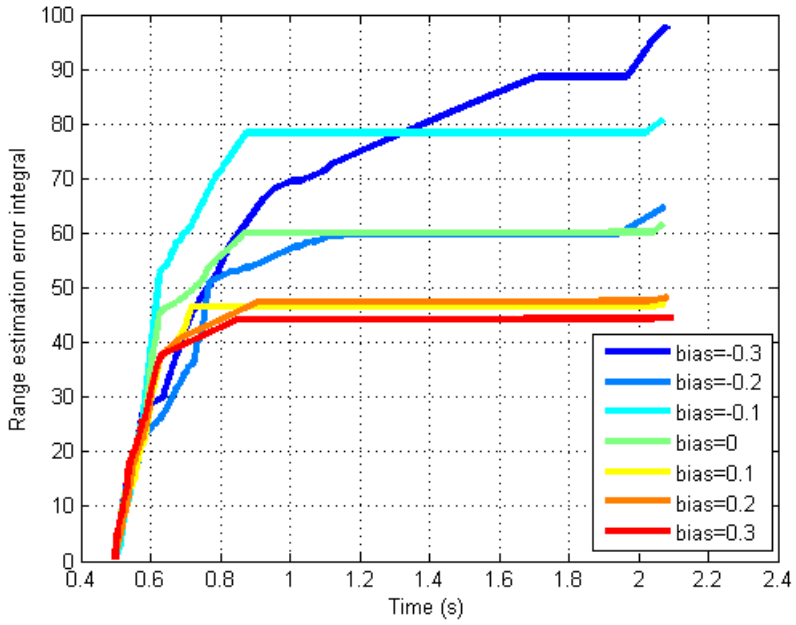

Figure 5.36. Integral of absolute range estimation error for different bias values

5.1.4. Non-Manoeuvring Missile

In the beginning of the thesis, it was stated that one of the strong suits of the proposed algorithm was that it can work even when the missile does not accelerate. For this case, a new set of scenarios are selected (Table 5.5). In this scenario set, the missile is fired as before, but not steered to its target, by setting PNG gain and bias zero.

The simulation is run with both IMU and seeker errors enabled. Moreover, since the missile is not expected to meet the target, the simulation termination condition is set 5 seconds.

Table 5.5. Scenario set #3

#	V_t (m/s)	γ_t (°)	x_{init} (m)	z_{init} (m)
1	200	20	500	50
2	100	240	2000	500
3	300	180	2000	500
4	0	0	1500	250

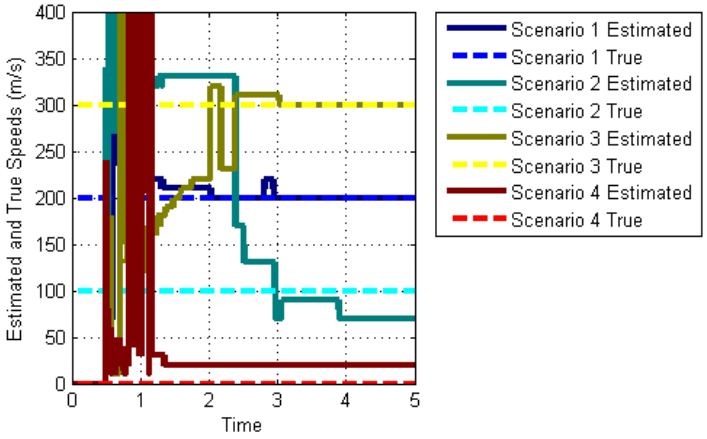

Figure 5.37. Estimated and true speeds for non-manoeuvring missile

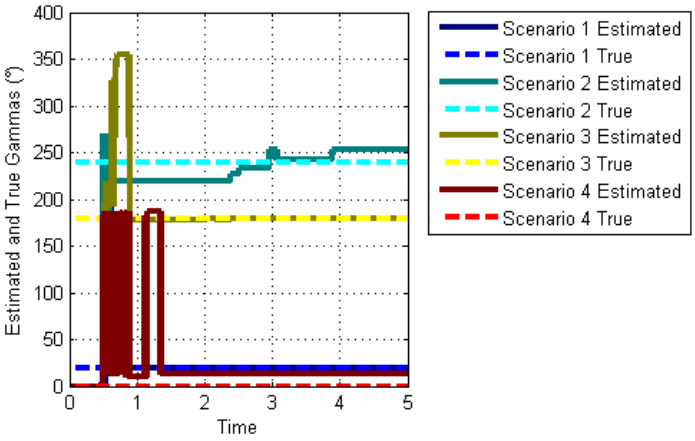

Figure 5.38. Estimated and true flight path angles for non-manoeuvring missile

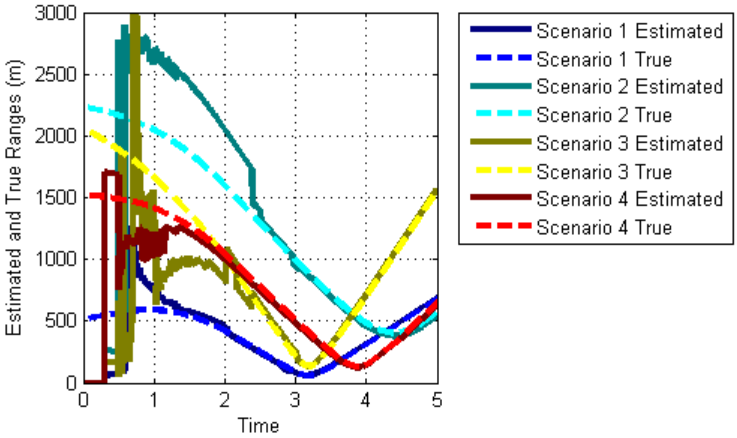

Figure 5.39. Estimated and true ranges for non-manoeuvring missile

Related results are plotted in Figure 5.37, Figure 5.38 and Figure 5.39. Note that, since the missile is not steered towards the target, range profiles start increasing after some point.

Immediate observation of the figures shows some deterrence in performance, but successful capture of the real parameters, similar to the previous cases, thus showing the performance of the algorithm when the missile does not manoeuvre.

5.2. Batch Run Simulations

In order to assess the performance of the algorithm within a broader space, it is tested in a batch run environment where the target velocity and initial position parameters are changed and they are shown in Table 5.6.

Table 5.6. Batch run parameters

	Selected increments
$\boldsymbol{\gamma_t}$ **(°)**	[0:45:315]
$\mathbf{V_t}$ **(m/s)**	[0:20:300]
$\boldsymbol{x_{init}}$ **(m)**	[500 1000 2000 4000 5000]
$\boldsymbol{z_{init}}$ **(m)**	[50 1000]

The selected increment size shown in Table 5.6 results in 1280 simulations which are intended to cover a variety of cases like close/far target or slow/fast target etc.

5.2.1. Determination of a Success Parameter for Batch Run

In order to assess the performance of the simulation, it is necessary (and easier) to visually compare the true and estimated parameters when a few scenarios are run (like in the section Individual Results). However, in this section, since there are many of them, visual comparison is impractical. Instead, a simple mathematical expression is used as shown in (5.2) where R denotes true range, $\hat{R}$ denotes estimated range, J denotes performance parameter and t_{total} denotes the total flight time.

$$J = \frac{1}{t_{total}} \int_0^{t_{total}} \left| R - \hat{R} \right| dt \tag{5.2}$$

However, starting the integration in (5.2) right from the beginning results in larger J values than expected since it would also include errors from the transient region. Therefore, the following workaround is applied in finding the J value:

- If the scenario takes less than 2 seconds, the integration is started upon initialisation of the algorithm.
- Otherwise, the integration is started at when the time reaches half of the flight time (e.g. if the missile takes 7 seconds to reach its target for a scenario, the integration is started at 3.5 seconds).

Moreover, a clear threshold J value must be selected for success criterion. After various individual runs, it could be said that a value of $J = 40\ m$ can be selected for a conservatively good target velocity and range estimation performance. To make this selection easy to comprehend (physically understandable), a sample run of which J is almost equal to 40 m (exactly 39.99 m). This run is obtained when the target moves with a speed of 80 m/s and an angle of 225°, starting from a location [4000 50] m. For this specific case, the range, speed and angle estimations are plotted in Figure 5.40, Figure 5.41 and Figure 5.42, respectively.

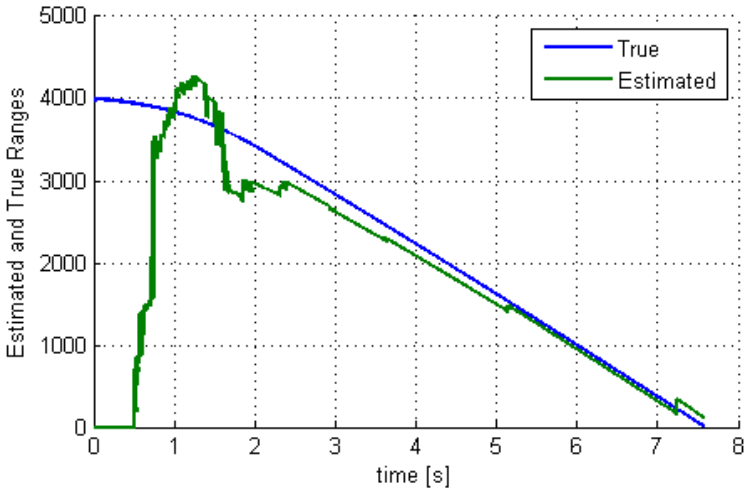

Figure 5.40. Sample range estimation performance having a performance parameter $J = 40\ m$

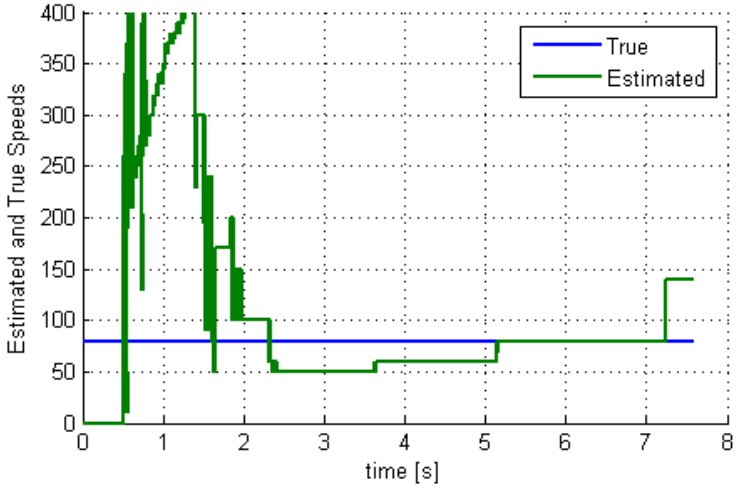

Figure 5.41. Sample speed estimation performance having a performance parameter $J = 39.99\ m$

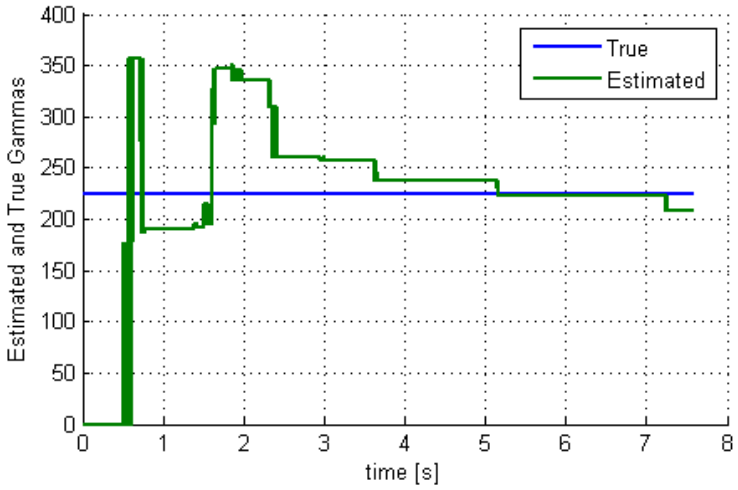

Figure 5.42. Sample target flight path angle estimation performance having a performance parameter $J = 39.99\ m$

Note that, in the aforementioned figures, it can be seen that, upon initialisation of the algorithm, the estimations take a bit of time to converge to its correct values, as expected.

While a J value of 40 is roughly selected for success criterion, success percentages for different J values are also shown in the Batch Run Results section.

5.2.2. Batch Run Results

As mentioned before, the batch run containing 1280 simulations with increments selected as in Table 5.6 is performed. When the batch run is performed under ideal conditions (no measurement noise or bias) all estimations become successful and therefore, their results are not included here.

Table 5.7. Success performances (case count when $J < J_{selected}$)

$J_{selected}$	1	5	10	25	40	75	100	500
Success (%)	34.84	42.5	49.141	63.51	76.88	88.75	91.48	99.84

When the same procedure is applied for non-ideal conditions, unsuccessful attempts are available. The success performance for different J values are presented in Table 5.7.

Also, the J values for changing γ_t and V_t values are plotted in Figure 5.43 and Figure 5.44 (Note that the colour scale for the two figures are different). One thing that can immediately be noticed is that, increasing initial range (further the target is) is detrimental to the performance, as the LOS rate gets is smaller as the range increases.

Also, the performance drops as targets escape with fast speeds due to the similar reasoning explained in the preceding paragraph.

All in all, it can be concluded that, for variety of scenarios and conditions, the proposed algorithm provides correct results with acceptable rates (namely 76.88% for a conservative J criterion).

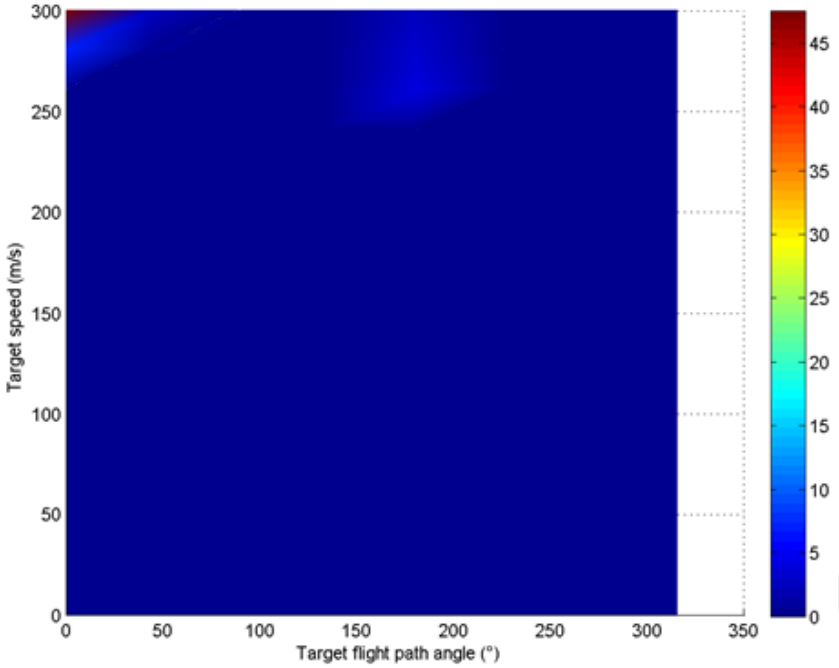

Figure 5.43. J values for different γ_t and V_t values where initial range of the target is 500 m

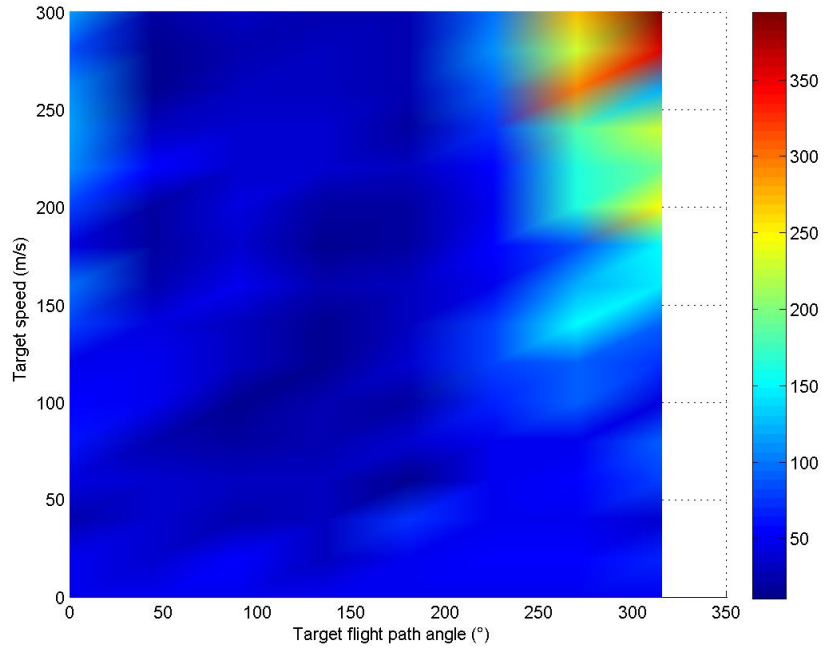

Figure 5.44. J values for different γ_t and V_t values where initial range of the target is 5100 m

5.3.Computational Time

One of the significant downside of the proposed algorithm is that it includes simple but numerous calculations, which requires significant amount computational time. In this section, effect of selecting the grid size of GPM to the computational time is analysed.

The analysis is performed by calculating the total simulation time for different increments of flight path angle and speed guesses. For the sake of this analysis, the $1/V_{t_{max}}$ rule is omitted and the increments are selected independently.

Table 5.8. Performance specifications of the computer

Specification	**Value**
CPU Frequency	2.4 GHz
# of CPU Cores	8
RAM	12 GB
Operating System	Windows 10, 64-bit
MATLAB Version	2017a

The simulations created in Simulink environment are run in *accelerator* mode with 1 milliseconds timestep and Euler integration. The specifications of the computer in which the simulations are performed are listed in Table 5.8.

Moreover, the scenario that has been used to assess the computational time is presented in Table 5.9.

Table 5.9. Computational time scenario

#	V_t **(m/s)**	γ_t **(°)**	x_{init} **(m)**	z_{init} **(m)**	**Engagement time (s)**
1	20	15	1000	50	3.069

Table 5.10. Selection of GPM increments for time analysis

	Selected increments
$\boldsymbol{\Delta\hat{\gamma}_t}$ **(°)**	[1, 2.5, 10, 20 ,45]
$\boldsymbol{\Delta\hat{V}_t}$ **(m/s)**	[5 10 20 50]

The engagement scenario depicted in Table 5.9 is run with different $\Delta\hat{\gamma}_t$ and $\Delta\hat{V}_t$ increments selected as in Table 5.10.

In the analysis, all combinations of selected increments are run. This means that, the total count of runs is $5 \times 4 = 20$. Using the selected increments depicted in Table 5.10, the search grid limits are selected as in Table 5.11.

Table 5.11. GPM limits used in time analysis

	Minimum	**Maximum**
$\boldsymbol{\hat{\gamma}_t}$ **(°)**	0	360- $\Delta\hat{\gamma}_t$
$\boldsymbol{\hat{V}_t}$ **(m/s)**	0	400

Consequently, minimum and maximum numbers of elements in the GPM becomes 72 and 29160, respectively. The simulation times with respect to each increment selection are plotted in Figure 5.45. Likewise, the simulation times with respect to total number of elements in the GPM are also plotted in Figure 5.46.

When both Figure 5.45 and Figure 5.46 are inspected, one can easily infer that a sharp change of computational time is present with the selection of increment size. Moreover, when a linear curve is fitted to Figure 5.46, (5.3) is obtained with an R^2 of 0.9972.

$$t_{sim} = 0.003562 GPMsize \tag{5.3}$$

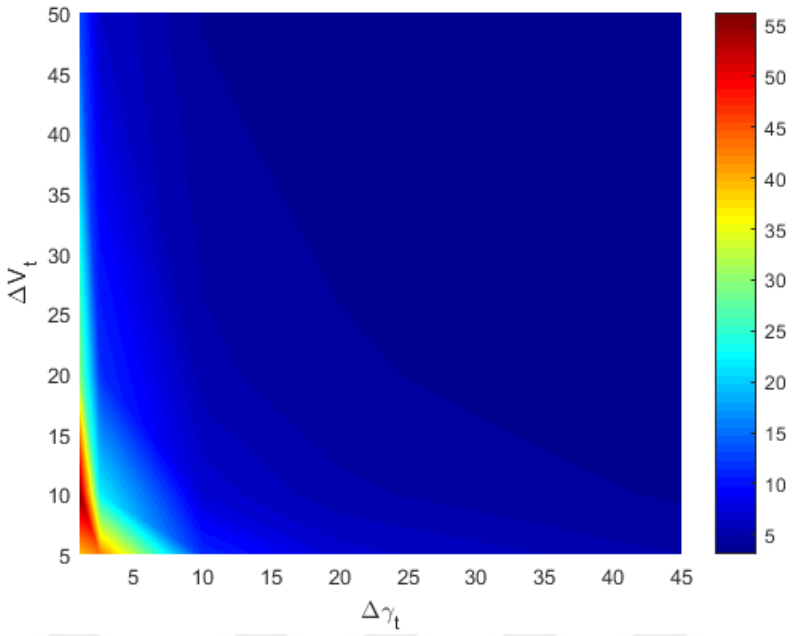

Figure 5.45. Resultant computational times (seconds) with respect to individual guess increments

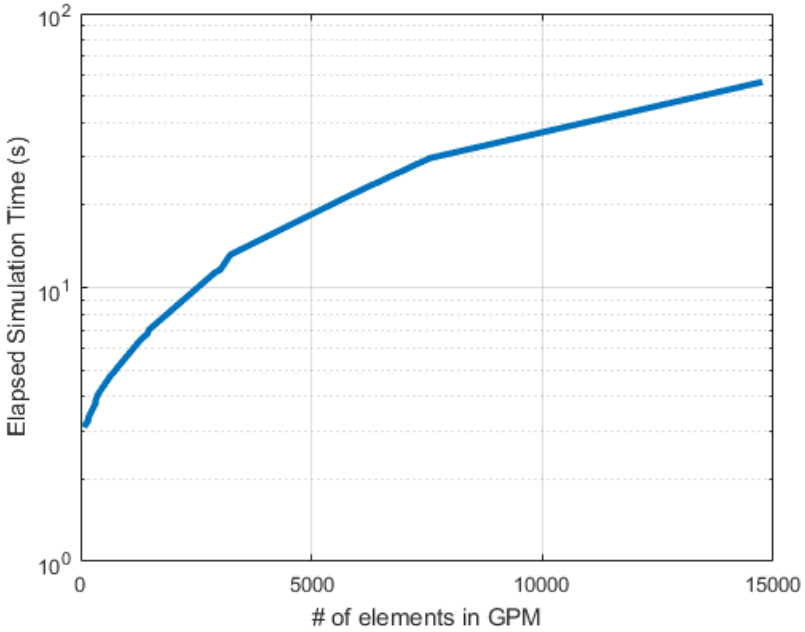

Figure 5.46. Resultant computational times (logarithmic scale) with respect to number of elements in GPM

(5.3) suggests that, the burden of each element in GPM is approximately 3.5 ms in a 3 seconds scenario. Consequently, with a GPM configuration used in previous

sections ($\Delta\hat{\gamma}_t = 2.5°$ and $\Delta\hat{V}_t = 10$ m/s), the number of elements in GPM becomes $144 \times 41 = 5904$; making the total run time of a 3 seconds simulation $0.009442 \times 5904 = 21.03$ seconds.

This phenomenon consists the biggest problem of the proposed algorithm. Possible theoretical remedies of this problem are proposed in the next chapter.

CHAPTER 6

CONCLUSION AND FUTURE WORK

In this chapter, some possible improvements to the algorithm are proposed. Then, a summary of the proposed algorithm and its results are presented.

6.1. Possible Future Work

Since the major drawback of the algorithm is its computational time (which is a function of the GPM grid), the proposed improvements to the algorithm focuses on decreasing the computational effort without decreasing observability. Instead of searching for the whole domain, the search grid can be optimised by certain methods. In this section, those possible optimization propositions are explained. Those propositions are:

- Selecting a nonuniform GPM grid
- Eliminating irrelevant elements in GPM
- An adaptive search algorithm, which starts from a coarser grid

6.1.1. Nonuniform GPM

Throughout the thesis a uniformly distributed GPM grid was used. That is, $\Delta\hat{\gamma}_t$ and $\Delta\hat{V}_t$ was constant. However, since errors related to these grids are dependent to each other, one can choose to have a nonuniform grid.

For example, if the target is slow, the observability of γ_t worsens, as it was shown in previous chapter. As a remedy, a finer grid of $\hat{\gamma}_t$'s can be selected corresponding to slow $\hat{V}_t$'s in order to increase observability in slower target speeds. Conversely, for large values of $\hat{V}_t$, a coarser $\hat{\gamma}_t$ grid can be chosen to save from computational time.

6.1.2. Irrelevant Elimination

Since an a priori information related to the target is unavailable, the algorithm should be initiated with a wide GPM range, including all possible scenarios. However, as the engagement occurs, some elements in GPM may become irrelevant to their scenarios.

To illustrate using the scenario set depicted in Table 5.1 are run with ideal measurements and the count of irrelevant scenarios are obtained. For this case, the following elements in the GPM are considered irrelevant:

(1) Those which has an altitude larger than 3 km

(2) Those which has a range larger than 7 km

(3) Those which have a negative range ($|\hat{\lambda}| > 90°$)

Since the same GPM composition as in Chapter 5 is used, it can be said that there is a total of 5904 elements in the GPM. The ones which are considered as irrelevant are summarised in Table 6.1.

Table 6.1. Irrelevant results (some elements may become irrelevant due to multiple reasons)

Scenario #	**1**	**2**	**3**	**4**	**5**	**6**
Total GPM	5904					
Total Irrelevant	5021	4277	4129	4112	5380	4607
Irrelevant by (1)	0	89	319	0	2377	1185
Irrelevant by (2)	0	0	5	0	4957	1284
Irrelevant by (3)	5021	4188	3810	4112	2880	3422
Irrelevant/Total ratio (%)	85.04	72.44	69.94	69.65	91.12	78.03

An examination of Table 6.1 suggests that, most of the elements in the GPM are actually irrelevant to their respective scenarios. This means that, one can save about 70% of computational time if the irrelevant elements are disregarded in estimation. However, lack of a priori information about the target forces the designer to start with

the broadest GPM domain possible as one cannot know the LOS/LOS rate profile beforehand to identify and eliminate the irrelevant elements.

Moreover, one can infer from Table 6.1 that the concept of irrelevance in this case is dominated by (3). Mathematically (3) means “negative range”. Physically, it means that the missile passed by that synthetic target, making that element irrelevant.

Another implication of Table 6.1 is related to the scenarios where the target is slow (5 and 6). If the target is slow, one can expect the LOS rate to be a small value. This forces the synthetic range calculations corresponding to high speed guesses to be large, making them irrelevant to the estimation. In Table 6.1, it can easily be seen that, fast scenarios did not produce any irrelevance due to (2) (except for a small number of 5 in scenario 3). Conversely, a significant number of irrelevance due to (2) can be observed in scenarios 5 & 6, owing to the aforementioned reason.

In Figure 6.1, Figure 6.2, Figure 6.3 and Figure 6.4 histograms (bin width: 0.5 s) of the time occurrences of irrelevance are plotted. The figures show the number of elements in the GPM which satisfies the irrelevance conditions, grouped by first time of occurrence.

The most prominent implication of the histograms is that, most of the first irrelevances occur at the initialisation of the algorithm (Figure 6.1). This could help the designer to eliminate the irrelevant elements before synthetic trajectory integration. However, that workflow may be insecure since the seeker measurement may be false at that specific time, leading erroneous results.

Similarly, the dominant characteristic of irrelevance due to negative range is also visible in the histograms. Upon initialisation, most of the elements become irrelevant. Afterwards, a small number of elements are added to the irrelevant pool as the engagement continues (Figure 6.4). This phenomenon occurs due to the fact that, as the engagement occurs, some of the synthetic trajectories passes by the missile, rendering them to have a “negative range”.

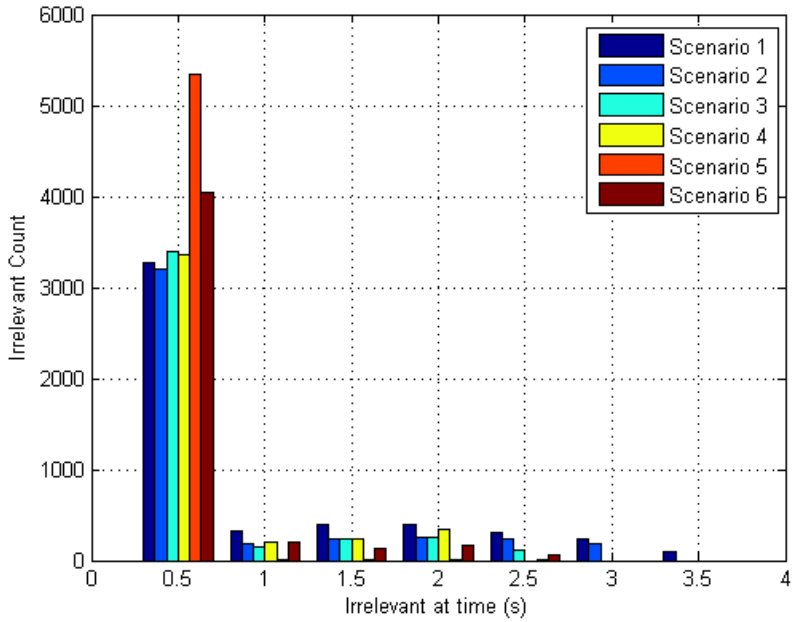

Figure 6.1. Histogram of irrelevant occurrence (any)

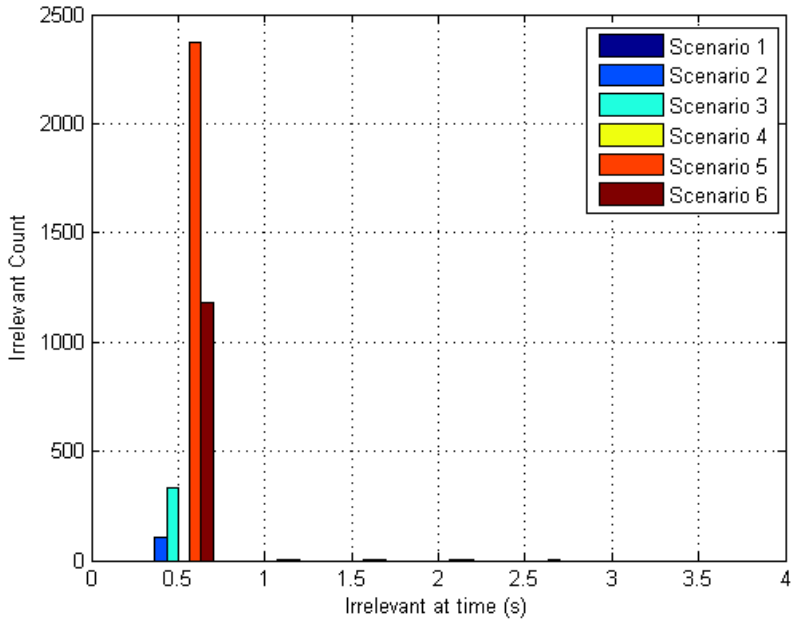

Figure 6.2. Histogram of irrelevant occurrence (Only by (1))

Moreover, parallel to the results shown in Table 6.1, in Figure 6.2 and Figure 6.3, the effect of irrelevance due to (1) and (2) on scenarios 5 and 6 can be seen. Other scenarios do not produce these irrelevance types much, as explained before.

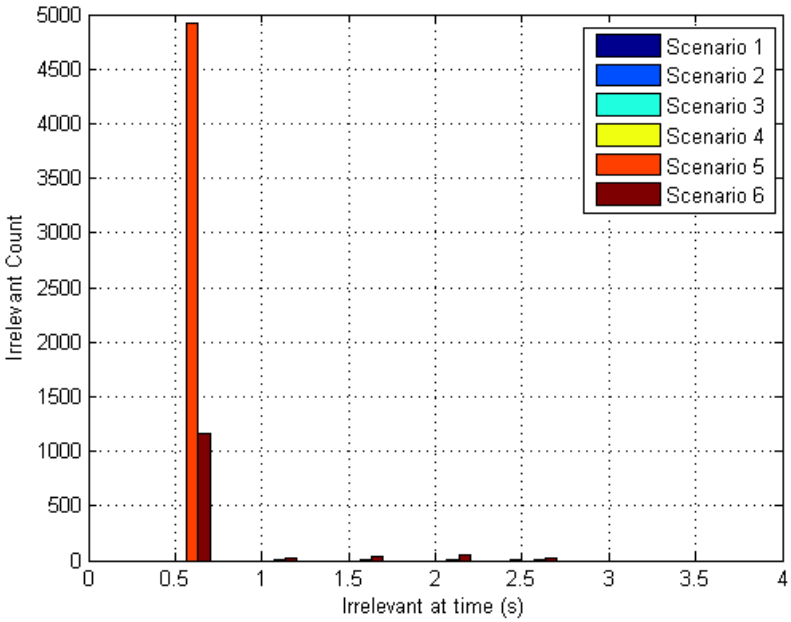

Figure 6.3. Histogram of irrelevant occurrence (Only by (2))

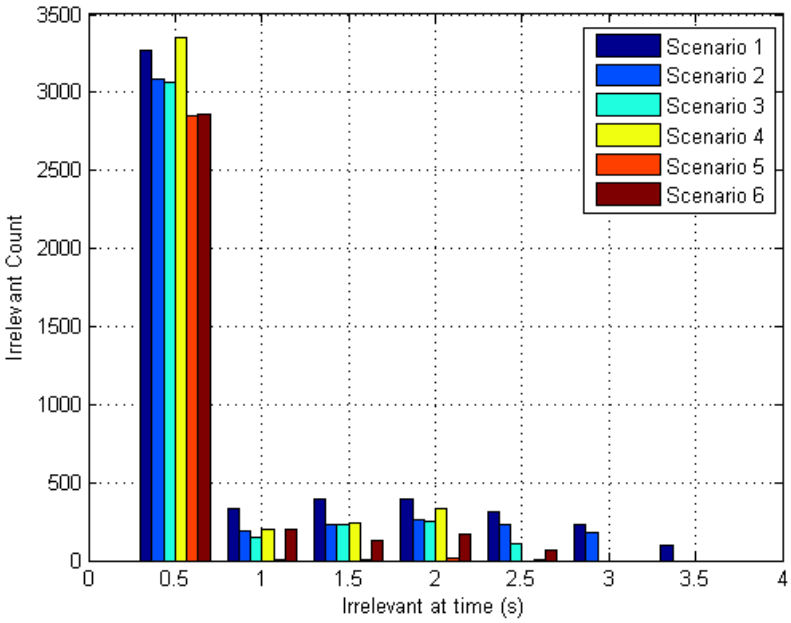

Figure 6.4. Histogram of irrelevant occurrence (Only by (3))

Likewise, as opposed to irrelevance due to (3), these cases are not added to the irrelevant pool conspicuously as the engagement continues. This can be explained by the fact that since the missile moves towards any synthetic target (except for negative range case), the engagement has the tendency to nullify the range. As this is the case,

if the synthetic range is within the specified limits prior to algorithm initialisation, it is unlikely to have an out-of-range value within the rest of the engagement.

6.1.3. Creating an Adaptive Algorithm

So far, the basis of the algorithm was to initialise the guesses by constructing a solid GPM grid throughout the engagement. It was also mentioned that this requires some computational time. One of the possible solutions for this problem is to start with a GPM and adapt it as the engagement proceeds.

One method that can be used could be is a *gradient based* algorithm like *steepest descend method*, where an initial guess is iterated through the steepest gradient until a performance parameter is satisfied. In gradient based algorithms, there is a risk of convergence to a *local minimum* rather than the *global minimum*. Therefore, it is very critical to select an initial guess that yields a global minimiser.

Likewise, other than gradient based algorithms, *global search algorithm* methods can be used. Such methods search the optimal solution within the entire set of possible solutions through an *objective function* and they do not need derivatives. Namely, in *particle swarm optimisation* (PSO), an initial guess and multiple particles are used. In that method, randomly generated points – called *particles* – are initiated and iterated until the optimisation criterion (e.g. a cost function) is minimised. Such a method may find the global minimum since it operates in the whole region as opposed to gradient based algorithms. However, the PSO may need some computational effort as it incorporates various particles to be iterated, depending on the selected particle count.

6.2.Conclusion

In this thesis, a new method for estimating target parameters and range-to-go without using standard Kalman Filters, which are susceptible to unobservability when the missile does not accelerate, is explained. It is explained that, each information related to the target and engagement is valuable for successful capture of the target; which is the basic motivation of estimating such parameters. Then, available methods within the literature for estimation are presented.

In the beginning, basic information related to missiles, missile algorithms and guidance are explained in order to familiarise the reader to the missile guidance

concept. For this purpose, elements in missile guidance & control and the control loop they establish is clarified. Concepts of autopilot & guidance are presented along with the engagement geometry that missile and target create, which is the basis of any guidance law. Also, equations related to engagement geometry are presented, which would be used in the algorithm.

Then, the algorithm is presented by starting with explaining the mathematics of the problem. The problem is approached by creating a grid called *Guessed Position Matrix* (abbreviated as GPM within the thesis) which includes all physically possible scenarios of the target. It is stated that at one timestep, the problem has infinitely many solutions; therefore, one should look for the solution to the problem within a time range. For that end, the *synthetic trajectories* concept is presented. By integrating the elements in the GPM, one can obtain a space of trajectories, one being the real case. Following that the problem evolves to selecting (or isolating) the true case among numerous trajectories. For isolation, the method of error integration (cost function) is described. That method includes calculating the LOS and LOS rates corresponding to each synthetic trajectory (called *synthetic LOS*/*LOS rate*) and comparing it with the real measurement. Clearly, the minimum error can be selected as the estimation.

Then the effects of errors in GPM to range estimation are examined. It could be seen that, the influence of errors to range estimation change with the target speed. Mathematically, it could be shown that, when the target moves slowly, the errors in flight path angle estimations has little effect onto range calculation; even though observability of flight path angle diminishes in this case. Conversely, if the target is fast, mathematical expression showed that the errors in flight path angle affect the range estimation greatly. Similarly, using the same expression, the grid selection of the GPM is forced to obey an equality.

After that, the environment that the algorithm would be tested was explained. The errors that were included in the system were presented along with defining the concepts of bias and noise. It is said that bias is a measurement error that would make the error of its integration larger as the time goes on. Conversely, noise does not diverge from the real integration; it rather deviates around it.

Then the results of the algorithm are presented starting with ideal results to validate the performance of the algorithm. The uniqueness problem could be seen, even when everything was ideal. The first meaningful estimations are obtained at the second timestep after the algorithm was initiated, proving the uniqueness problem. Then the scenarios are run under non-ideal conditions (IMU & Seeker Error with Non-Element case) to assess the robustness of the algorithm. It is seen that, for slow targets, the observability of the flight path angle worsens. Nevertheless, since the speed estimations are good enough, the range estimations are not greatly affected by flight path angle estimation. Conversely, when the target is fast, a small error in flight path angle affected the range estimation more, in conjunction with the previous assertions regarding the mathematical expression that relates estimation errors with range estimation. It is also seen that observability of flight path angle is better in a fast target scenario, which improves the range estimation for this case.

Following those analyses, the effect of guidance parameters to the performance of the algorithm is explained. For that analysis, different PNG gains and bias values are selected for a specific scenario, of which estimation performance are investigated by looking for the integral of the errors in range estimations. It is seen that, conditions where the engagement become slow (namely low PNG gains), the performance of the algorithm worsens as the observability of the engagement diminishes.

Then the performance of the algorithm when the missile does not manoeuvre, which was one of the benefits of the proposed algorithm, is investigated. To that end, some scenario conditions are run where the missile does not accelerate, and the measurements are contaminated with errors. It is asserted that, the algorithm works under those conditions, which could be advantageous for missiles with a midcourse phase where missile acceleration is mostly close to null.

Subsequently, the algorithm is tested in a broader space, in order to numerically demonstrate that the algorithm performs well in the whole working domain. While it is mentioned that the algorithm works perfectly under ideal circumstances; when errors are introduced to measurements, a success criterion seemed to be necessary to assess the performance. Consequently, it is stated that with the selected criterion – a rather conservative one – the success rate of the algorithm is found as 76.875%. It

could also be argued that the type of engagement is the most critical element for convergence. It is seen that engagements resulting in low LOS rate values during initialisation of the algorithm, depreciates the performance significantly.

Moreover, since the algorithm requires a lot of calculations and integration, the required computational time for a specific scenario was also analysed. It was seen that, each element in the GPM increases the computational time by nine milliseconds in a three seconds simulation.

Finally, some possible solutions for the computational time are proposed. Those include nonuniform GPM, irrelevant elimination and an adaptive algorithm. In nonuniform GPM case, since the observability of the system changes with target speed, it was proposed that, one can choose to change the GPM grid size with target speed. In irrelevant elimination, it is possible to eliminate any physically infeasible cases and continue the estimation with the remaining elements in the GPM; hence the improvement the computational time. Also, one can find a clever solution such that, the algorithm changes its grid size during flight.

BIBLIOGRAPHY

[1] R. Yanushevsky, Modern Missile Guidance, Boca Raton, Florida: CRC Press, 2008.

[2] N. A. Shneydor, Missile Guidance and Pursuit, Chichester, West Sussex: Horwood Publishing Limited, 1998.

[3] R. Chavarriaga, T. Strösslin, D. Sheynikhovich and W. Gerstner, "A Computational Model of Parallel Navigation Systems in Rodents," *Neuroinformatics,* vol. 3, no. 3, pp. 223-241, 2005.

[4] N. F. Palumbo, "Guest Editor's Introduction: Homing Missile Guidance and Control," *Johns Hopkins APL Technical Digest,* vol. 29, no. 1, pp. 2-8, 2010.

[5] P. Zarchan, Tactical and Strategic Missile Guidance, vol. 176, Reston, Virginia: American Institute of Aeronautics and Astronautics Inc., 1997.

[6] N. F. Palumbo, R. A. Blauwkamp and J. M. Lloyd, "Modern Homing Missile Guidance Theory and Techniques," *Johns Hopkins Apl Technical Digest,* vol. 29, no. 1, pp. 42-59, 2010.

[7] I.-S. . Jeon, J.-I. . Lee and M.-J. . Tahk, "Impact-time-control guidance law for anti-ship missiles," *IEEE Transactions on Control Systems and Technology,* vol. 14, no. 2, pp. 260-266, 2006.

[8] J.-I. . Lee, I.-S. . Jeon and M.-J. . Tahk, "Guidance law to control impact time and angle," *IEEE Transactions on Aerospace and Electronic Systems,* vol. 43, no. 1, pp. 301-310, 2007.

[9] K. S. Erer and K. Özgören, “Control of Impact Angle Using Biased Proportional Navigation,” in *AIAA Guidance, Navigation and Control Conference*, Boston, 2013.

[10] L. G. Taff, “Target localization from bearings-only observations,” *IEEE Transactions on Aerospace and Electronic Systems*, vol. 33, no. 1, pp. 2-10, 1997.

[11] R. . Stansfield, “Statistical theory of d.f. fixing,” , 1947. [Online]. Available: http://digital-library.theiet.org/content/journals/10.1049/ji-3a-2.1947.0096. [Accessed 7 9 2017].

[12] H. E. Daniels, “The Theory of Position Finding,” *Journal of the Royal Statistical Society*, vol. 13, no. 2, pp. 186-207, 1951.

[13] K. . Dogancay and G. . Ibal, “3D passive localization in the presence of large bearing noise,” , 2005. [Online]. Available: http://ieeexplore.ieee.org/xpl/freeabs_all.jsp?arnumber=7077977. [Accessed 8 9 2017].

[14] D. Simon, “Kalman Filtering,” *Embedded Systems Programming*, pp. 72-79, June 2001.

[15] G. Welch and G. Bishop, “An Introduction to the Kalman Filter,” University of North Carolina at Chapel Hill, Chapel Hill, 2001.

[16] B. F. L. Scala, M. . Mallick and S. . Arulampalam, “Differential geometry measures of nonlinearity for filtering with nonlinear dynamic and linear measurement models,” *Proceedings of SPIE*, vol. , no. , p. , 2007.

[17] B. Friedland, “Optimum Steady-State Position and Velocity Estimation Using Noisy Sampled Position Data,” *IEEE Transactions on Aerospace and Electronic Systems*, vol. 9, no. 6, pp. 906-911, November 1973.

[18] A. . Nordsjo, “A constrained extended Kalman filter for target tracking,” , 2004. [Online]. Available: http://ieeexplore.ieee.org/document/1316407. [Accessed 8 9 2017].

[19] V. J. Aidala, “Kalman Filter Behavior in Bearings-Only Tracking,” *IEEE Transactions on Aerospace and Electronic Systems,* vol. 15, no. 1, pp. 29-39, January 1979.

[20] J. M. Passerieux and D. V. Cappel, “Optimal observer maneuver for bearings-only tracking,” *IEEE Transactions on Aerospace and Electronic Systems,* vol. 34, no. 3, pp. 777-788, 1998.

[21] V. J. Aidala and N. C. Steven, “Observability Criteria for Bearings-Only Target Motion Analysis,” *IEEE Transactions on Aerospace and Electronic Systems,* vol. 17, no. 2, pp. 162-166, 1981.

[22] S. E. Hammel and V. J. Aidala, “Observability Requirements for Three-Dimensional Tracking via Angle Measurements,” *IEEE Transactions on Aerospace and Electronic Systems,* Vols. AES-21, no. 2, pp. 200-207, March 1985.

[23] T. L. Song, “Target adaptive guidance for passive homing missiles,” *IEEE Transactions on Aerospace and Electronic Systems,* vol. 33, no. 1, pp. 312 - 316, January 1997.

[24] T. L. Song and T. Y. Um, “Practical guidance for homing missiles with bearing-only measurements,” *IEEE Transactions on Aerospace and Electronic Systems,* Vols. AES-32, no. 1, pp. 434-443, 1996.

[25] W. Bell and S. Hillmer, “Initializing the Kalman Filter for Nonstationary Time Series Models,” Bureau of the Census, Washington D.C., 1987.

[26] Oxford Living Dictionaries, “Oxford Living Dictionaries,” Oxford University Press, [Online]. Available: https://en.oxforddictionaries.com/definition/missile. [Accessed 8 September 2017].

[27] G. M. Siouris, Missile guidance and control systems, New York, NY: Springer, 2004.

[28] K. S. Erer and O. . Merttopçuoglu, “Indirect Impact-Angle-Control Against Stationary Targets Using Biased Pure Proportional Navigation,” *Journal of Guidance Control and Dynamics*, vol. 35, no. 2, pp. 700-704, 2012.

[29] N. F. Palumbo, R. A. Blauwkamp and J. M. Lloyd, “Basic Principles of Homing Guidance,” *Johns Hopkins Apl Technical Digest*, vol. 29, no. 1, pp. 25-41, 2010.

[30] Honeywell International Inc., “HG1930 Inertial Measurement Unit,” 2016. [Online]. Available: https://aerospace.honeywell.com/en/~/media/aerospace/files/brochures/n61-1637-000-000-hg1930inertialmeasurementunit-bro.pdf. [Accessed 02 10 2017].